SOME DESIGN ASPECTS OF THE MULTI FLUX BARRIER ROTOR RELUCTANCE SYNCHRONOUS MACHINE

Xola B. Bomela

Thesis presented in partial fulfilment of the requirements for the degree of Master of Science in Electrical Engineering at the University of Stellenbosch, South Africa.

Supervisor: Dr Maarten J. Kamper, University of Stellenbosch

December 2000

Declaration

I, the undersigned, hereby declare that the work contained in this thesis is my own original work and that I have not previously in its entirety or in part submitted it at any university for a degree.

Xola B. Bomela

Date: 21 November 2000

Abstract

This thesis deals with different design aspects of the multi-flux barrier rotor of the reluctance synchronous machine (RSM). The effect of the different designs on the performance of the RSM is investigated by means of two-dimensional finite element analysis. The finite element analysis is also directly used in the optimum design of the rotor of the RSM. The importance of the use of the finite element analysis in the design and performance calculations of the RSM is illustrated in this thesis.

The design aspects of the RSM which are focussed on in this thesis are, amongst other things, the chording of the stator winding, the skewing of the rotor and the ratio of the number of rotor flux barriers to the number of stator slots of the RSM. The effects of these design aspects on the average torque and torque ripple of the RSM are investigated and general design directives are given. The occurrence of flux pulsations in the stator teeth and rotor iron segments of the RSM are also studied to some extent.

The finite element optimum design of a 4-pole RSM-rotor with a high number of flux barriers is described in the thesis. This optimum designed rotor is built and the RSM with this rotor is tested in the laboratory. Its calculated and measured performances are studied and compared with a conventional, low number rotor flux barrier RSM. It is found, amongst other things, that the RSM with the high number of rotor flux barriers has a slightly higher average torque with a significantly lower torque ripple.

Opsomming

Hierdie tesis handel oor verskillende ontwerp-aspekte van die reluktansie sinchroonmasjien (RSM) met 'n multi-vloedversperringsrotor. Die effek van die verskillende ontwerpe op die vermoë van die RSM is met behulp van twee-dimensionele eindige element analise ondersoek. Die eindige element analise is ook direk in die optimum ontwerp van die rotor van die RSM gebruik. Die belangrikheid van die gebruik van die eindige element analise in die ontwerp en vermoë-berekening van die RSM word in die tesis geïllustreer.

Die ontwerp-aspekte van die RSM waarop in hierdie tesis gefokus word, is onder andere die spoel-steekverkorting van die statorwikkeling, die skuinsing van die rotor en die verhouding van die getal rotor-vloedverperrings tot die getal statorgleuwe van die RSM. Die effek van hierdie ontwerp-aspekte op die gemiddelde draaimoment en draaimoment-rimpel van die RSM word ondersoek en algemene riglyne vir die ontwerp van die RSM word gegee. Die voorkoms van vloedpulsasies in die statortande en rotor yster segmente van die RSM word ook deels ondersoek.

Die eindige element optimum ontwerp van 'n 4-pool RSM-rotor met 'n hoë getal vloedversperrings word in die tesis beskryf. Hierdie optimum ontwerpte rotor is gebou en die RSM met hierdie rotor is in die laboratorium getoets. Die berekende en gemete vermoë is bestudeer en vergelyk met die vermoë van 'n RSM met 'n konvensionele, lae getal vloedversperrings rotor. Dit is onder andere gevind dat die RSM met die hoë getal rotor-vloedversperrings 'n effens hoër gemiddelde draaimoment het met 'n behuidende laer draaimoment-rimpel.

Acknowledgements

I would like to express my sincere appreciation to:

- My study leader, Dr Maarten Kamper, for his supervision and constant support and encouragement, and also his unmeasurable efforts to ensure the availability of financial assistance for the project.
- LIW, a division of Denel, of which I am the employee, for providing financial assistance.
- All the student colleagues from the Electrical Machines Group and the technical staff of the electrical machines workshop for their interest and support.
- The Centre for Mechanical Services (SMD) for the assembling and testing of the prototype system.
- My family, in particular my mother for her keen interest and motivation to finish this thesis research with success.
- My God, my Lord Whom I know has been with me through out my studies. Praise His holy name.

Contents

List of Figures

List of Tables

List of Principal Symbols

A_z	magnetic vector potential in the z-direction; **Wb/m**
a_{sc}	active copper area of a stator conductor; **m²**
$\hat{B}$	flux density vector; **Wb/m²**
B_d, B_q	*d*- and *q*-axis flux densities; **Wb/m²**
B_{mt}, B_{my}	maximum tooth and yoke flux densities, respectively; **Wb/m²**
b_p or bp	flux barrier pitch; **m**
b_w or bw	flux barrier width; **m**
c	coil span in terms of number of slots per pole
d_i	stator inner diameter; **m**
E_a	rms value of the phase EMF; **V**
g_d, g_q	resultant airgap lengths of the *d*- and *q*-axis magnetic circuits; **m**
I_s	rms phase current; **A** with **rad**.
$\hat{I}_s$	magnitude of the current space phasor; **A**
i_d, i_q	*d*- and *q*-axis stator current components; **A**
J	current density; **A/m²**
K	general machine constant
k_{w1}	winding factor for the fundamental
l	core length; **m**
L_e	endwinding leakage inductance; **H**
L_{dm}; L_{qm}	*d*- and *q*-axis magnetising inductances; **H**
L_d; L_q	*d*- and *q*-axis synchronous inductances; **H**
m	number of phases
M_t; M_y	teeth and stator yoke iron masses, respectively; **kg**
m	gradient in the flux barrier width and barrier number relation

n_a	number of parallel circuits
n_b or nb	number of flux barriers
n_{sl}	number of stator slots
p	number of poles
P_{cu}	given copper loss; **kW**
q	number of slots per pole per phase
rh	rib height; **m**
R_c	per phase core loss resistance; Ω
R_s	per phase stator resistance; Ω
T	torque; **Nm**
λ_d, λ_q	*d*- and *q*-axis fundamental stator flux linkage components, **Wb**
λ_s	space phasor of stator flux linkages, **Wb rad**
λ_{abc}	instantaneous values of total flux linkages of phases a, b and c; **Wb**
α	skewed angle by which the submachines are displaced
ϕ	angle between current space phasor and rotor d-axis; **rad**
ω_r	electrical speed of rotor reference rame; **rad/s**

Abbreviations:

FE	**F**inite **E**lement
FEM	**F**inite **E**lement **M**ethods
RSM	**R**eluctance **S**ynchronous **M**achine

Chapter 1

Introduction

Reluctance Synchronous Machines (RSMs) are increasingly being an interest of research subject as they could be considered as the alternative to its counterparts, namely permanent magnet, switched reluctance and induction machines. It has been shown by research that the RSM has at least the same and higher power density than the induction machine in the low and medium power level. Reluctance machines, and specifically the reluctance synchronous machine, offer certain advantages which make them very attractive for, amongst other things, the use in traction applications.

1.1 The reluctance synchronous machine

The RSM is an AC machine with a standard, non-salient, three-phase stator and an unexcited rotor with magnetic asymmetry or saliency. The RSM generates torque and, hence, develop mechanical power due to the magnetic saliency of the rotor. No windings, brushes or permanent magnets are used on the rotor which makes the RSM a simple and robust electric machine. This machine is a type of synchronous machine. Current research shows that the optimum designed RSM under current vector control, i.e. using an inverter and a closed-loop control system, has attractive torque and efficiency characteristics [1], [2].

RSMs have the following advantages over permanent magnet machines:

(i) there is no concern with demagnetisation, hence RSMs are inherently more reliable than permanent magnet machines;

(ii) the excitation field of the machine can be adjusted, thus, allowing field weakening for high speeds;

(iii) RSM rotors, except axially laminated types, can be constructed entirely from high-strength, low-cost materials.

RSMs can be used when several motors must operate in synchronism for coordinating machines and where a wide range of highly regulated speed control is required with a variable frequency drive. Some of the other applications for RSMs are in traction and wheel drives and generally in fan and pump drives.

1.2 The research background on RSM

Recently the research work on reluctance machines took a new direction due to the advent and intensive use of power electronics. Not to mention the direct application of the FE software to design and optimise the overall reluctance synchronous machine (both the stator and rotor). This has taken a significant forward step in advance design of the RSM generally. Recent research has also shown that the current controlled RSM has a good power density, in contrast to the RSMs which operate from fixed mains frequency and voltage supplies. It must be noted that the good power density of this machine was made possible by the use of the closed-loop switching. This means that the rotor position and the phase current are fed back and the current is spatially placed in the machine according to the position of the rotor.

The research work done on the RSM recently at the University of Stellenbosch can be summarised as below and referring to Figure 1.1. This figure shows four RSM rotors with internal flux barriers. The RSMs with these rotors have been designed, built and tested at the Electrical Machine Research Laboratory of the University of Stellenbosch. These RSMs range from small to medium and post 100kW power machines .

The significance of these machines is that FE methods were used for the design optimisation of the machines. Their design optimisation procedure as well as the FE calculated and measured results are comprehensively discussed in [1]-[5] and [16]-[17]. Figure 1.1(a) shows an 8-internal flux barrier RSM rotor proposed by Honsinger [31] and studied further and built by Kamper (1994) [29]. The rotor in Figure 1.1(b) was optimum designed by Kamper (1996) for a 9 kW RSM in a 5.5 kW induction machine frame. It was found that the good power density and high efficiency of the RSM obtained from this design in the small (sub 10 kW) power range, were clearly the most advantages of the RSM [5].

The RSM-rotor developed for a wheel drive application is shown in Figure 1.1(c). It is for a medium

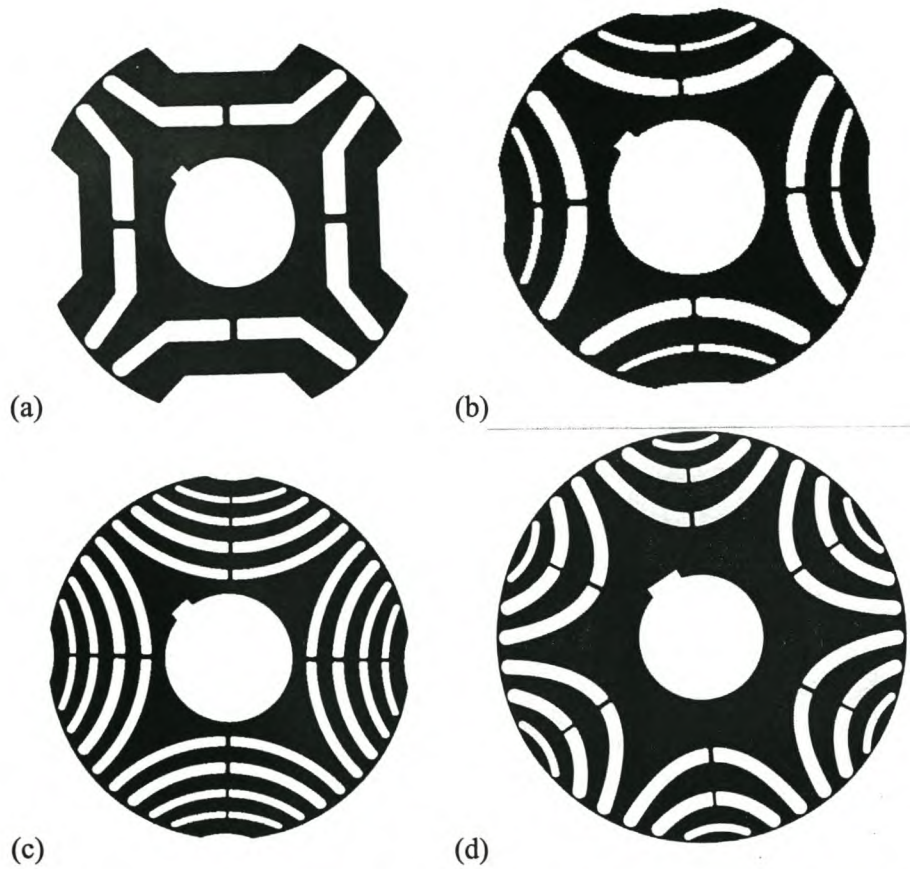

Figure 1.1: Rotors used in the research on RSMs: (a) Kamper(1994), (b) Kamper (1996), (c) Bomela (1998) and (d) Germisshuizen (1999).

power (sub 50 kW) RSM which was built and tested in a 37 kW induction machine frame. The performance results of this RSM are discussed in [2]. For a rail traction application, the 110 kW RSM-rotor of Figure 1.1(d) was developed. This rotor is optimum designed with two-dimensional FE software and optimisation algorithms. The intention is to use this machine as a traction motor for suburban locomotives and to compare the performance of a 110 kW induction locomotive traction motor with that of a reluctance synchronous traction motor. This 30-flux-barrier, six pole rotor was optimum designed, built and tested by Germisshuizen (1999) [17].

1.3 Thesis objective

The objective of the thesis is to obtain some general design directives for the design of the RSM. This is done by investigating the effects of some of the design aspects of the RSM on the average

torque, torque ripple, power factor and the efficiency of the machine.

1.3.1 Problem statement

Despite the recent research on the design of the RSM there are still rising questions on some of the design aspects of the machine. The first question is what effect does the stator winding chording and rotor skew have on the average torque and torque ripple of the RSM, and is there an optimum stator chording and optimum rotor skew for the machine? The second question is what effect does the ratio of the number of stator slots to the number of rotor inner flux barriers have on the average torque, torque ripple and flux pulsations in the machine. The flux pulsations in the stator teeth and rotor iron are important to investigate as they affect the stray load losses and efficiency of the machine.

1.3.2 Approach to problem

As the first step to answer the questions raised in section 1.3.1 the finite element (FE) analysis was used to vary the stator chording and rotor skew of two RSMs with their rotors shown in Figures 1.1(b) and (c). The advantage of using these RSM-rotors is that they were already built and available. The FE analsysis was also used to study the effect of the ratio of the number of rotor flux barriers to the number of stator slots on the performance of the RSM by varying the ratio. As a result of this analysis a 64-flux barrier rotor RSM was built, run and tested. This was done to comparatively study the overall FE calculated and measured results of the RSMs with low and high number of rotor flux barriers. The high number of flux barrier rotor was optimum designed using the FE method directly in the optimisation procedure.

1.4 Thesis layout

The layout of the thesis is as follows:

Chapter 2: The RSM mathematical model is briefly discussed with the steady-state d- and q-axis equivalent circuits and space phasor diagram of the RSM. The significant relationships between the flux and current, and the torque and current are discussed. The power factor of the machine is analytically described as well.

Chapter 3: The aim of this chapter is to optimise machine dimensions to maximise the performance output of the machine through FE analysis and the optimisation algorithms. The focus of this design methodology is on small to medium power RSMs.

Chapter 4: In this chapter specific attention is given to the effect of chording the stator winding and skewing the rotor on the average torque and, most importantly, the torque ripple of the machine.

Chapter 5: The effect of the rotor flux barrier to stator slot ratio on average torque and torque ripple of the machine is investigated and discussed in this chapter. A brief discussion of the flux pulsations in the RSM is also presented.

Chapter 6: This chapter discusses the calculated and measured results of the three RSMs studied. These are the chorded plus skewed 32-flux barrier rotor RSM; the single layer unskewed 32-flux barrier rotor RSM and a single layer unskewed 64-flux barrier rotor RSM.

Chapter 7: In this chapter a summary with conclusions is given and recommendations are made for further research.

Chapter 2

RSM Mathematical Model

This chapter describes the equivalent circuit parameters of the RSM. The approximate steady-state *dq* equivalent circuits of the machine in the rotor reference frame, and space phasor diagrams are given to explain the flux-current and torque-current relationships and also to explain the power factor of the machine.

2.1 Equivalent circuits and phasor diagram

The approximate steady-state *d*- and *q*-axis equivalent circuits and phasor diagram of the RSM in the rotor reference frame are shown in Figure 2.1. The *d*-axis is normally chosen in the direction of largest permeance. The flux linkages λ_d and λ_q are the *d*- and *q*-axis stator flux linkage components, which include the stator leakage flux linkage but not the endwinding leakage inductance L_e. The parameters R_s and R_c are respectively the per phase winding resistance and per phase core loss resistance. R_s is calculated from the active copper area available at a temperature of 120^oC ($\Delta T + T_{ambient}$). The active copper area available is determined from the given slot dimensions. The formula for the per phase stator winding resistance is

$$R_s = \frac{2W\rho_t\,(l + l_e)}{n_a A_{cu}/z} \tag{2.1}$$

where l_e is the average length of a coil-end, n_a is the number of parallel circuits and A_{cu}/z is the active copper area of a stator conductor, ρ_t is the resistivity of copper at a temperature t_c and is given by $\rho_t = \rho_{20}\,(1 + Y_t(t_c - 20))$. The $\rho_{20} = 17 * 10^{-9} ohm.m$ and $Y_t = 0.0039/^0C$.

It is necessary to specify the current $\mathbf{I_s} = \hat{I}_s \angle \phi$ of the machine, to calculate the flux linkage using the FE method. Due to the fact that the RSM is under direct current control, the current space phasor

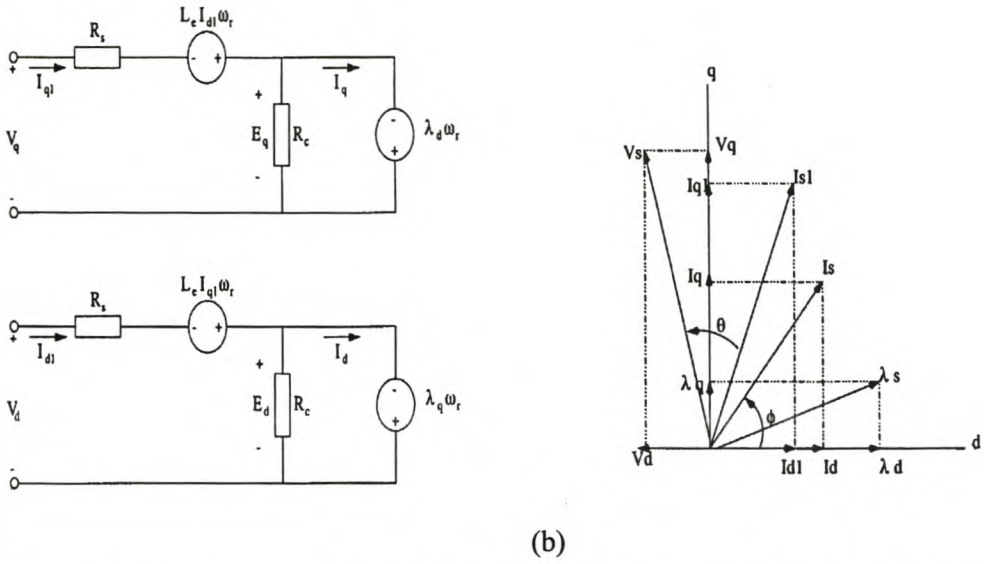

(a) (b)

Figure 2.1: (a) Steady-state d- and q-axis equivalent circuits and (b) space phasor diagram of the RSM [5].

$\mathbf{I_s}$ can be set at an angle ϕ with respect to the rotor as shown in Figure 2.1. The amplitude of the current space phasor, $\widehat{I}_s$, is determined from either a given *rms* current density J as given by

$$\widehat{I}_s = \sqrt{2} J a_{sc} n_a, \tag{2.2}$$

where $a_{sc} = A_{cu}/z$ is the active copper area of a stator conductor, or from a given copper loss P_{cu}, as given by

$$\widehat{I}_s = \sqrt{2P_{cu}/(3R_s)} = C n_a \sqrt{P_{cu} a_{sc}} \ . \tag{2.3}$$

With the current space phasor known in terms of amplitude and angle, the dq current components and the instantaneous three-phase currents, I_{dq} and i_{abc} respectively, can be calculated using the inverse Park's transformation. To calculate the total three-phase stator flux linkages λ_{abc} that exclude the endwinding flux linkage, the FE analysis method is used. With the total phase flux linkages and the rotor position known, the dq flux linkages of Figure 2.1, λ_d and λ_q, can be calculated using Park's transformation. From this, the speed voltages of the equivalent circuits can be determined.

The only remaining parameter, R_c, can be determined as [1], [5]

$$R_c = 3\frac{E_a^2}{P_c} \quad , \tag{2.4}$$

where E_a, the *rms* value of the phase EMF, is given by $E_a = \frac{1}{4}\sqrt{(E_d^2 + E_q^2)}$. P_c, the iron core losses, is calculated as $P_c = cf_1^x(B_{mt}^y M_t + B_{my}^y M_y)$, where B_{mt} and B_{my} are respectively the maximum flux densities in the teeth and yoke. These can be obtained directly from the FE solution. M_t and M_y are the iron masses of the teeth and yoke respectively and f_1 is the fundamental supply frequency. The constants c, x and y were determined from measurements on electrical machines and also from the loss-frequency curves of the laminations used. These constants, for this analysis, are taken as $c = 7.5$, $x = 1.32$ and $y = 2$ [5].

With all the equivalent circuit parameters calculated, the dq currents I_{dq1} and supply current I_{s1} are determined, followed by the calculation of the dq supply voltages. The power factor and the steady-state torque of the RSM in the rotor reference frame are respectively calculated by Equations (2.13) and (2.7) as explained in the next sections.

2.2 Flux-current relationship

The flux-current relationship of the RSM is one of its important characteristics. When this relationship is linearised as shown in Figure 2.2(a), it can simply be expressed as

$$\begin{bmatrix} \lambda_d \\ \lambda_q \end{bmatrix} = \begin{bmatrix} L_d & 0 \\ 0 & L_q \end{bmatrix} \begin{bmatrix} i_d \\ i_q \end{bmatrix}. \tag{2.5}$$

For example, the equation $L_d = \lambda_d / i_d$ (see Figure 2.2) can be used to determine the d-axis synchronous inductance.

On the other hand, the relationship must in general be written as in Equation (2.6), where θ is the rotor angle with respect to the stator. The flux variation with θ is caused by the variation in the airgap flux which varies due to the mutual position of the stator teeth and rotor iron segments.

$$\lambda_d = f(i_d, i_q, \theta) \; and \; \lambda_q = f(i_d, i_q, \theta) \tag{2.6}$$

The non-linear relationship between d-axis flux and d-axis current is due to saturation and is common in all electrical machines. Concerning the q-axis magnetic circuit, the non-linearity between flux and

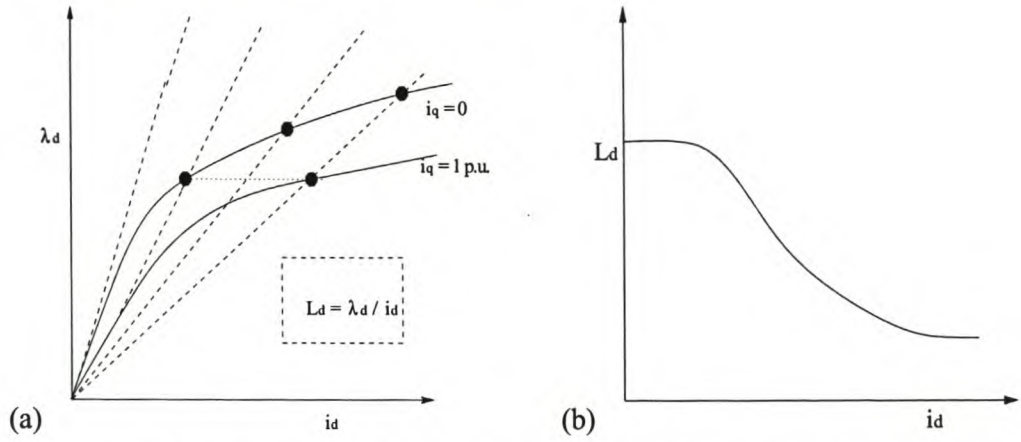

Figure 2.2: Typical relations of d- axis flux linkage, inductance and current relation of the RSM.

current is caused mainly by the small iron ribs and webs of the rotor which saturate. Furthermore, magnetic cross-coupling appears in Equation (2.6). The dependence of λ_{dq} on i_{qd} represents the well-known armature-reaction effect in electrical machines [8], i.e. the d-axis flux is affected by the q-axis current and the q-axis flux is affected by the d-axis current.

It is thus clear from Figure 2.2 and Equations (2.5) and (2.6) that the inductances L_d and L_q of the RSM vary with current. Equations (2.7) and (2.15) show that the performance of the RSM is very dependent on these inductances .

The FE analysis of the flux-current relationship of the RSM, where cross magnetisation and saturation effects are taken into account, is well discussed in a number of publications, amongst others, [5] and [29].

2.3 Torque-current relationship

The three-phase stator winding and the three-phase currents of a reluctance machine create a rotating magnetic field in the air-gap of the machine. A so-called reluctance torque is developed because the magnetic field created in the rotor will cause the rotor to align and run synchronously with the rotating stator field. From this, thus, the name reluctance synchronous machine.

To produce the reluctance torque, the RSM must be designed such that the stator winding inductances vary with the position of the rotor. Figure 2.3 shows a cross sectional view of a RSM which consists of a three-phase nonsalient stator and a salient pole rotor. In the figure, a three-phase stator winding is shown, although a higher number of phases can also be used. Notice that the inductance of each stator phase winding varies with rotor position such that the inductance is a maximum when the

rotor axis is aligned with the magnetic axis of that phase and a minimum when the two axes are perpendicular.

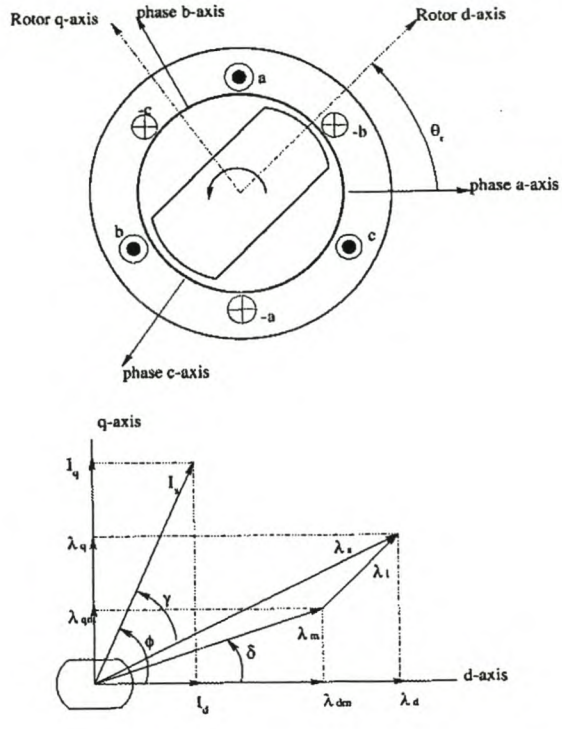

Figure 2.3: Basic three-phase RSM and space phasor diagram.

Explaining the figure briefly further, the angle θ_r is the electrical rotor angle between the magnetic axis of phase a and the d-axis of the rotor. The reference frame rotates at an electrical speed of $w_r = \frac{d\theta_r}{dt}$. The fundamental current and flux linkage space phasors of the machine, I_s and λ_s respectively (see Figure 2.3), are stationary with respect to each other and with respect to the rotor in the steady-state. In the figure, γ is the torque angle, which is zero when the current space phasor lies either on the d- or q-axis of the rotor.

The steady-state torque of the RSM can be expressed in terms of the dq-axis components for a p pole-pair machine as derived in all classical texts on dq-axis theory as

$$T = \frac{3}{4}p(L_d - L_q)\widehat{I}_s^2 \sin(2\phi) \ , \tag{2.7}$$

where L_d and L_q are the d- and q-axis inductances of the machine due to the d- and q-axis airgap fundamental stator flux linkage components. It is clear that the torque of the RSM is a function of

the inductance difference $(L_d - L_q)$, the *rms* phase current I_s and the current space phasor angle ϕ. From Equation (2.5) the inductances of Equation (2.7) are given by

$$L_d = \frac{\lambda_d}{I_d} \tag{2.8}$$

$$L_q = \frac{\lambda_q}{I_q} \,. \tag{2.9}$$

The inductance difference $\Delta L = L_d - L_q$ of Equation (2.7) is not a constant but varies with both the d- and q-axis currents of the machine due to saturation and cross magnetisation [29]. This is explained in the previous section and by Equation (2.6). In effect the inductance difference is a function of the *rms* phase current I_s for a given current space phasor angle ϕ, i.e. $\Delta L = f(I_s,\ \phi)$. Hence, for a given ϕ Equation (2.7) can be written as :

$$T = K\Delta L\hat{I_s}^2 \,, \tag{2.10}$$

where $K = \frac{3}{4}p\sin(\phi)$ is a general constant of the machine. For a given current space phasor angle, ϕ, it seems from Equations (2.7) and (2.10) that the relation between torque and *rms* phase current is quadratic. Though, in contrast, it is found from measured and FE calculated results (see Chapter 6) that this relation is more linear due to the variation of ΔL in Equation (2.10).

2.4 Power factor

The reluctance synchronous machine is typified by having a rotor whose structure is such that the inductance of the stator windings vary from a maximum value L_d (direct inductance) to a minimum value L_q (quadrature inductance) as a function of angular displacement of the rotor. A figure of merit for the RSM is the ratio of the direct inductance to the quadrature inductance, $\frac{L_d}{L_q}$.

By using the phasor diagram of Figure 2.1(b) and by ignoring the stator and iron loss resistances in the equivalent circuits of the RSM (Figure 2.1(a)), the power factor of the machine can be expressed as [3], [5]

$$pf = \cos(\arctan(\frac{\frac{v_d}{v_q} + \frac{i_d}{i_q}}{1 - \frac{v_d}{v_q}\frac{i_d}{i_q}})) \tag{2.11}$$

$$= \cos(\arctan(\frac{\frac{L_q i_q}{L_d i_d} + \frac{i_d}{i_q}}{1 - \frac{L_q}{L_d}})) \quad , \tag{2.12}$$

and by multiplying through by $\frac{L_d}{L_q}$, Equation (2.12) becomes:

$$pf = \cos(\arctan(\frac{\tan(\phi) + \frac{L_d}{L_q}\frac{1}{\tan(\phi)}}{\frac{L_d}{L_q} - 1})) \; . \tag{2.13}$$

For a given current space phasor angle ϕ, e.g. $\phi = 45^0$, the optimal power factor angle is obtained by differentiating Equation (2.13) and equating to zero. Theoretically, if saturation and cross magnetisation are ignored, the optimal angle of the power factor results to

$$\theta_{optimal} = \tan^{-1}\left(\sqrt{\frac{L_d}{L_q}}\right) \; . \tag{2.14}$$

Thus, the maximum power factor can be expressed as below after substituting the angle $\theta_{optimal}$ in Equation (2.13):

$$pf_{max} = \frac{\frac{L_d}{Lq} - 1}{\frac{L_d}{Lq} + 1} \; . \tag{2.15}$$

Higher $\frac{L_d}{L_q}$ ratios yield higher power factors, and reduced volt-ampere ratings of the inverter powering the machine. This means that L_q must be relatively small as the power factor is sensitive to the value of L_q. From Equation (2.15) the power factor of the RSM, in contrast with the torque, is dependent on the inductance ratio which is also not a constant due to saturation and cross magnetisation. As in the case of the inductance difference, the inductance ratio $\sigma = \frac{L_d}{L_q}$ is a function of the *rms* phase current I_s (from Figure 2.1) for a given current space phasor angle ϕ, i.e. $\sigma = f(I_s)$.

Chapter 3

Design Methodology

The aim of this chapter is to describe and explain the optimisation of the machine dimensions of the RSM to maximise the performance output of the machine. The optimisation procedure makes use of FE analysis and optimisation algorithms. The focus of this design methodology is on small and medium power RSMs. Figure 3.1 already shows an example of a medium power, 4-pole, multi-flux barrier rotor RSM.

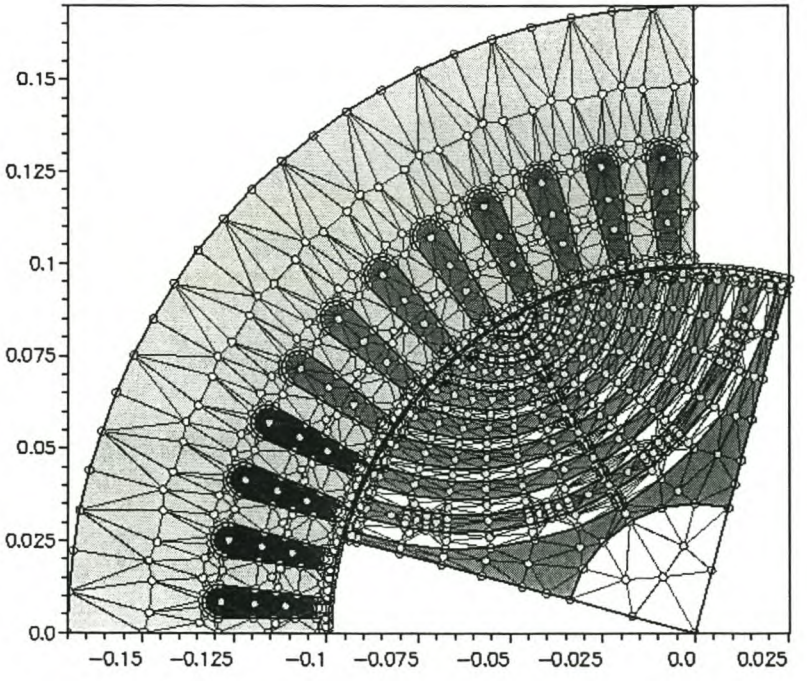

Figure 3.1: Meshed RSM pole.

3.1 Finite element analysis

The 2-D finite element package used in the design of the RSM is not of the commercial use. This package has been developed at Cambridge University, United Kingdom. The source code is available which enables one to use and program it for the FE analysis of any electrical machine. Some of the program extracts are given in Appendices B and C. The FE program makes use of triangular elements of the first order. Only one pole of both the stator and the rotor of the RSM is meshed with one airgap element comprising nodes on both sides of the airgap. A meshed pole with nodes (stator and rotor) of a RSM is shown in Figure 3.1.

In Figure 3.2 the procedure is given of how the performance parameters of the RSM are calculated. The machine dimensions, X, must be specified to run the program so that the performance parameters, Y, of the machine like torque, power factor, efficiency, etc. can be calculated. When the program runs, some subroutines are called to make it possible to calculate these performance parameters. These subroutines are shown in Figure 3.2. The FE program with these subroutines is called Solve (see Appendix C). The program can be run either in an interactive session or as background task which enable the user to exit from the session with the job running in the background. This is a common approach for most of the larger FE modelling packages. Brief explanations of the

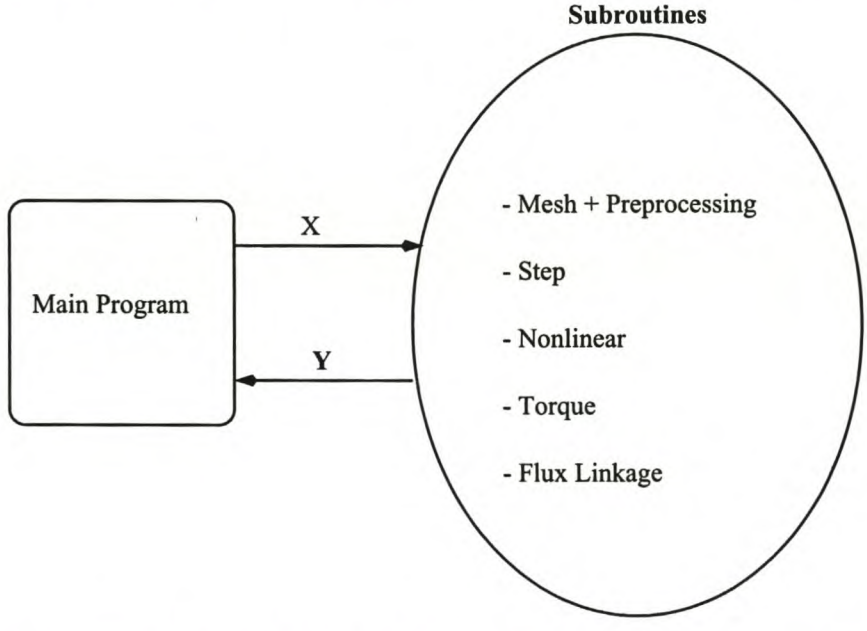

Figure 3.2: Simple procedure to calculate RSM performance parameters by FEM

subroutines of Figure 3.2 are as follows:

- **Mesh and preprocessing:** The accuracy of the FE solution is dependent on the mesh topology and attention should be placed in creating it. Essentially there are two types of mesh generators. The first being an analytical mesh generator that defines the problem geometry using large global elements. These global elements are subsequently refined according to the user, usually automatically. The other type of mesh generator, which is the one used in this thesis, is a synthetic generator where the user designs a mesh region at a node by node level and the model is the union of a number of different mesh regions. Modern commercial finite element packages generate the mesh automatically from the geometric outline of the problem drawn in a CAD type package. Automating the mesh generation drastically reduces manpower costs.

  Only one quarter of the rotor of the RSM is outlined in terms of xy-coordinates and meshed and mirrored to other quarters to make a full rotor. The same applies to the stator where only one stator slot of the machine is outlined, meshed and mirrored to the number of stator slots over a full pole pitch. See Figure 3.1 for the meshed RSM pole and the program in Appendix B. Thereafter, the phase windings are allocated to the respective slots. The stator and the rotor are then joined, followed by the preprocessing to save storage and calculation time. The numbering of the equations is optimised to minimise the solution time. The concern that rises during the meshing process is the possibility of the mesh elements to be distorted or changed in shape as the dimensions of the machine change during the optimisation. This will negatively affect the accuracy of the results. However, this was never experienced.

- **Step subroutine:** The air-gap element is a macro element that replaces the air-gap mesh and, therefore, is a convenient way of modelling rotor movement. Stepping the rotor is possible with no new mesh generation required. A time saving computational scheme is used, which enables rapid re-calculation of the air-gap element stiffness matrix. This subroutine determines the new stiffness matrix terms for the stepped air-gap element.

- **Nonlinear subroutine:** The Newton-Rhapson solution procedure is used by this subroutine to perform a nonlinear solution. It calculates the magnetic vector potentials at the different nodes (magnetic vector potential nodes). It is a solution of nonlinear equations due to the nonlinearity of the magnetic materials used. This means that the effects of saturation and cross magnetisation are taken into account.

- **Torque subroutine:** The torque subroutine calculates the torque from the vector potential nodal values in the air-gap at each rotor position. The air-gap vector potential values are obtained from the nonlinear solution. The torque subroutine has an integer variable that is set to calculate the torque harmonics up to this given integer. For instance, with the integer set at

one, only the (average torque) fundamental component of the torque is calculated.

- **Flux linkage subroutine:** The total stator flux linkage of each of the three-phase windings of the stator windings is calculated using this subroutine. Since this is a two dimensional FE solution, the calculated flux linkages include the main and stator leakage flux but not the end-winding leakage flux. An empirical formula is used to calculate the end-winding leakage inductance.

The computation time per FE program solution depends on the number of finite elements used in the mesh. The ribs and webs of the RSM multi-flux barrier rotor (see Figure 3.3) are meshed with a relatively high number of elements . This is necessarily due to the fact that the level of saturation at these parts of the rotor is high and it affects the output performance of the machine. The meshing of ribs and webs is shown in Figure 3.3 (a) and (b). The ribs and webs are respectively the iron segments between the machine airgap and the flux barrier tips as shown in Figure 3.3(c), and the small iron segment that divides the flux barrier into two, also shown in Figure 3.3(d). The relatively high number of elements required, thus, for the FE modelling of the RSM negatively affects the computation time. It is found that with an average of 3320 elements and 1892 nodes per pole of the RSM, the computation time per FE program solution on a Pentium II Processor 233 MHz is between 3 to 4 minutes.

Finally, Figure 3.4 shows the typical flux lines of the FE solution. In the figure, the rotor q-axis is aligned with the magnetic phase a-axis, and both the d- and q-axis currents are flowing in the machine.

3.2 Skew

The skewed rotor in the 2-D FE model can be represented by a number of two dimensional slices each at a different position. Each slice is displaced by an angle called the skew angle, α, along the axis of the skewed rotor. This representation of skew is shown in Figure 3.5.

The FE analysis as described in section 3.1, takes the 2-D slices as a set of unskewed sub-machines which are relatively displaced by the skew angle. This technique is discussed in several other publications such as [1] and [5]. For example, having k submachines, the flux linkages are calculated by Equation (3.1), where $\lambda_{abc}(\beta_n)$ denotes the total phase flux linkages of the unskewed machine with the rotor at position β_n.

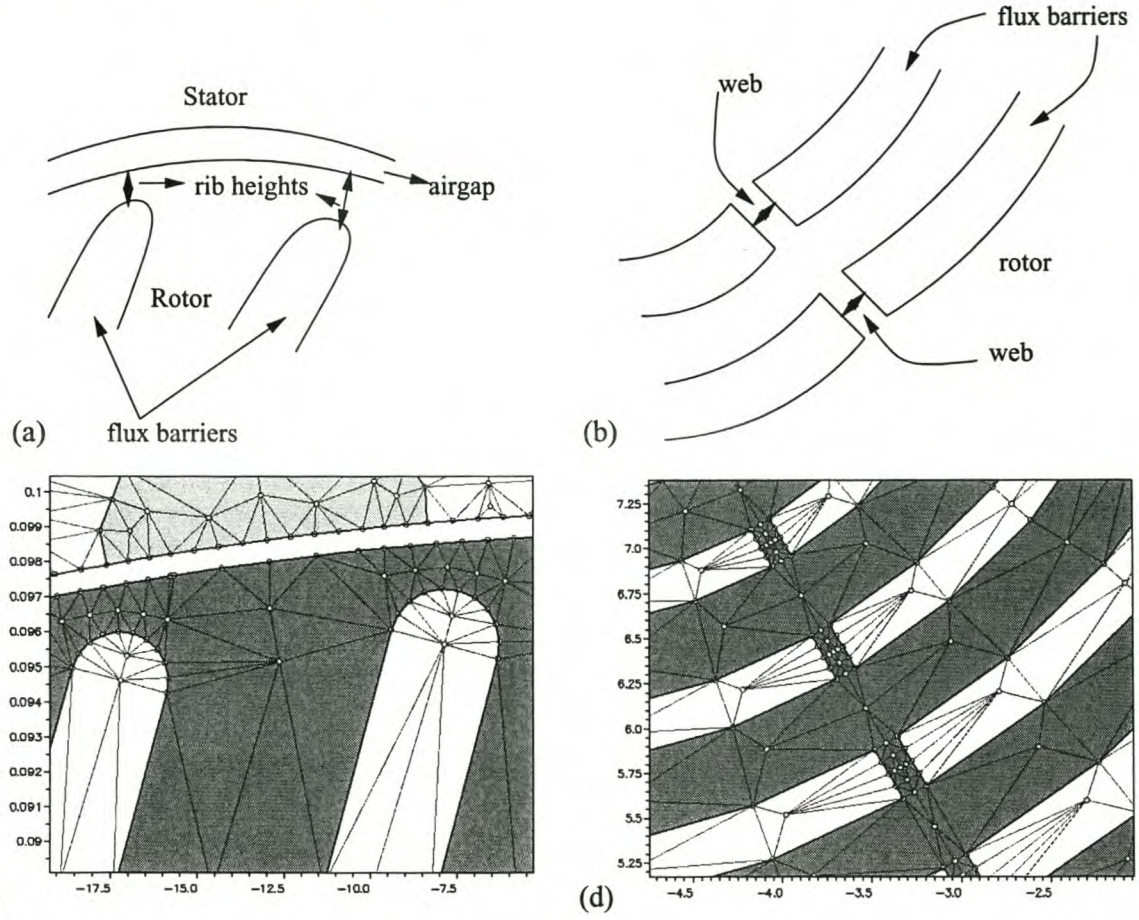

Figure 3.3: Schematic drawings showing rotor ribs (a) and webs (b), and meshed rotor ribs (c) and webs (d).

$$\lambda_{abc} = \frac{1}{k} \sum_{n=1}^{k} \lambda_{abc}(\beta_n) \ . \tag{3.1}$$

Simirlary to the calculation of the flux linkages, the torque for each submachine n and the average torque of the whole skewed machine with k slices can be calculated respectively by using Equations (4.10) and (4.11).

Equation (3.1) suggests that k time-expensive FE field solutions are required, but it is only the first non-linear solution at position β_1 which will take time due to the unknown reluctivities. At positions β_2, ..., β_k, the known reluctivities of previous positions can be used, which will already be close to the new reluctivities, so that the field solution time at these positions will be less. It is found that with $k = 5$ the skewed rotor is well represented in the FE analysis [1]. With $k = 1$ the rotor is

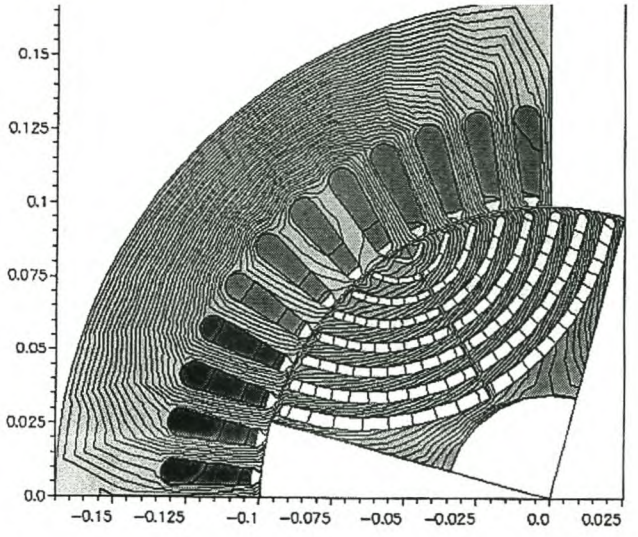

Figure 3.4: FE field plots

considered unskewed.

3.3 Finite element design optimisation

With the power and speed of workstations available today it is possible to use the FE model of the RSM in the optimisation procedure directly. This approach is used in this thesis for the design optimisation of the machine. The FE solution is particularly important in the design analysis of the RSM. It gives very accurate calculated results and takes into account the cross magnetisation

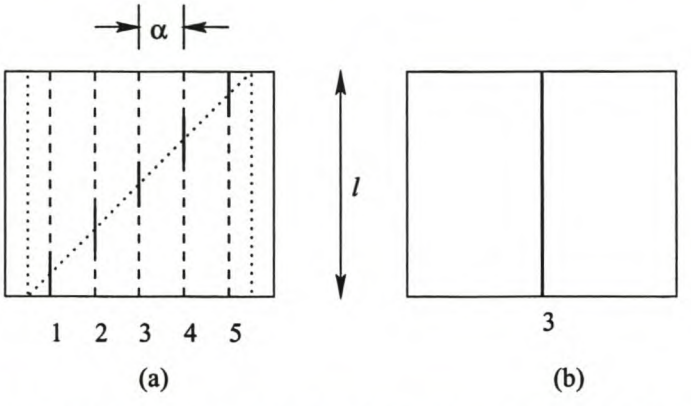

Figure 3.5: Representation of a skewed machine with k submachines (a) and unskewed machine (b).

and saturation effects. This is in contrast to the commonly used lumped circuit model which does not give absolute optimisation results. The use of the FE program in the design optimisation can basically be explained by the flow diagram of Figure 3.6 [1].

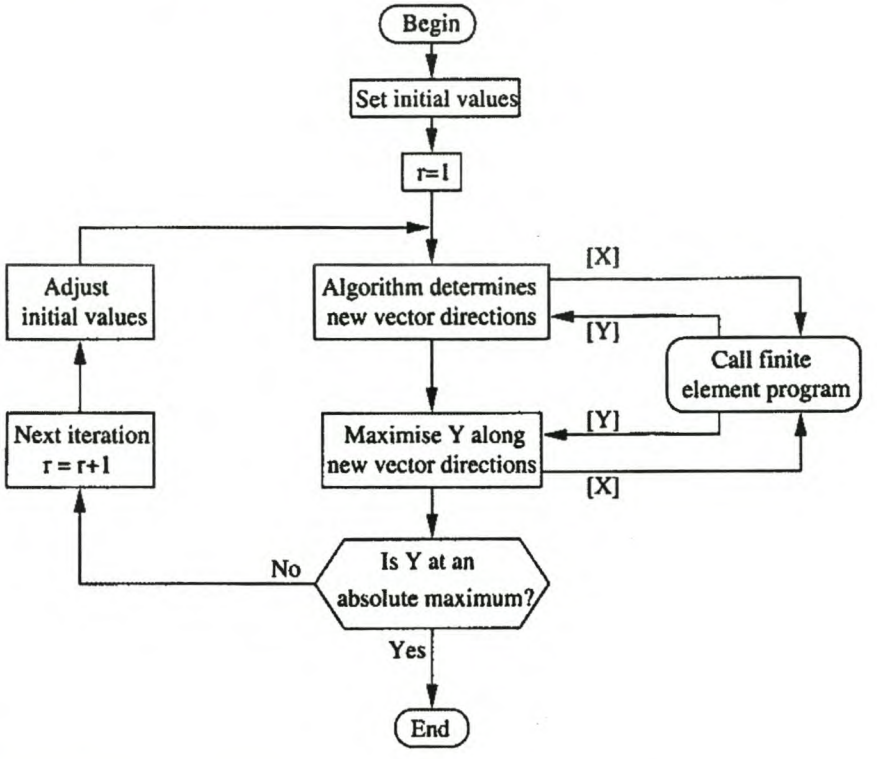

Figure 3.6: Basic optimisation procedure using the FE solution directly [1].

The flow diagram shows that the optimisation algorithm finds the values of the machine variables, *X*, that maximise the performance parameter of the machine. Note that the FE program is only used to calculate the performance parameter, *Y*, needed by the optimisation algorithm. In this process with each iteration *r* the algorithm determines directions of search in a multidimensional space along which the performance parameter of the machine is maximised. A new mesh is generated according to the changed input dimensions, *X*, (i.e. the values of variables of the machine) each time the FE program is called to calculate the performance parameter. The program then does the preprocessing and the nonlinear solution to find the magnetic vector potentials. The flux linkages and flux densities are then calculated, followed by the calculation of the output performance parameters of the machine, *Y*, e.g. torque, power factor, efficiency, etc.

The FE program may be called for a number of times by the algorithm during an iteration. At the end of each iteration a test is made to determine if an absolute maximum or minimum is reached.

If not, a next iteration is executed. With the high power and speed of the computer used, this time consuming process will be overcome. This also means that the mesh generation, preprocessing and the solving of the vector potentials must be an accurate and fast process. The optimisation algorithm must be fast as well.

3.4 Design optimisation of a 64-flux barrier RSM rotor

The optimisation procedure of section 3.3 is used to optimise the design of a 4-pole, 64-flux barrier rotor using a 48-slot stator. The rotor is shown in Figure 3.8, while the stator is shown in Figure 3.9. Kamper (1998) [2] in his design used the same stator as in Figure 3.9, but with a different rotor namely a 32-flux barrier plus cutout rotor (see Figure 1.1(c)). The stator has an unchorded single layer winding in 12 stator slots per pole.

The aim of the optimisation is to optimise the design of the 64-flux barrier rotor in the same 48-slot stator of Kamper (1998) [2]. The reason for the latter is to compare the performance of the 64-flux barrier rotor with the 32-flux barrier rotor with a cut-out of Kamper (1998) shown in Figure 1.1(c). Another reason for the latter was to investigate particularly the stator tooth and rotor iron segment flux pulsations of the medium power RSM. Depending on the rotor design, high frequency pulsations can occur in the stator teeth and iron segment of the RSM. Consequently, the iron losses increase and the efficiency of the machine drops.

In the design optimisation of the rotor of Figure 3.8 only the flux barrier widths are varied. The web widths and rib heights are not varied. These are taken as thin as mechanically possible in the analysis. Of course, they must comply with mechanical exigencies. A rule of thumb for the punching of the lamination is to make the widths and heights of the saturated iron bridges (webs and ribs) not less than the thickness of the lamination itself [5]. From this and from mechanical strength analysis (rotor speed at 3000 *rpm*), the web widths and rib heights are as specified in Table 3.1.

To keep the design optimisation of the flux barrier widths simple, the optimisation was based on a linear relationship between the widths of the different flux barriers. This linear relationship is illustrated for example in Figure 3.7. According to this relationship the width of a flux barrier is given by

$$bw(n) = [m(n-1)+1] * w \quad , \tag{3.2}$$

where m is the gradient of the linear relationship (Figure 3.7), $bw(n)$ is the width of the nth flux-barrier ($n = 1, 2, 3, ..., 8$ is this case) and w is also a width equal to $bw(1)$. So, instead of optimising

Table 3.1: Some dimensions of the 64-flux barrier rotor of Figure 3.8 (widths and heights are in *mm*; angles in *degrees*)

Flux-Barrier	Web widths	Rib heights	Flux-barrier widths	Fixed Flux-barrier angle
1	2.1	1.4	4.41	5.625
2	1.8	1.4	3.99	16.875
3	1.5	1.2	3.59	21.875
4	1.2	1.2	3.18	24.000
5	1.2	1.2	2.77	28.125
6	1.0	1.0	2.36	31.875
7	1.0	1.0	1.95	35.000
8	-	1.0	1.54	39.375

eight variables, Equation (3.2) makes it simple to optimise only two variables namely the gradient m and the flux barrier width, w.

From the optimisation process the gradient m resulted negative as shown in Figure 3.7. This im-

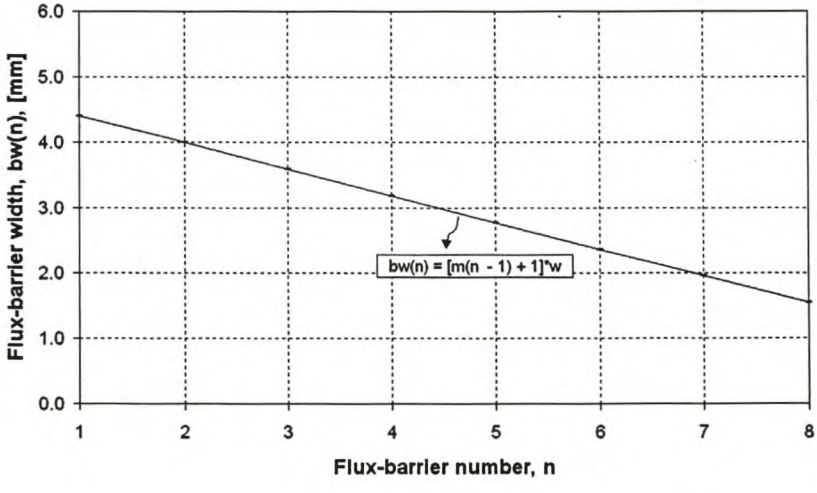

Figure 3.7: Barrier width (in *mm*) *versus* barrier number (see also Figure 3.8).

plies that the flux-barrier width decreases from the first flux barrier to the eighth flux barrier as shown in Figure 3.8. The reason for this is that the peak value of the sinusoidal distributed stator MMF is close to the middle of the rotor-pole, i.e. close to the first number of flux barriers of the rotor of Figure 3.8. The latter is so due to the relatively high current angle of typically 65^o which causes the q-axis MMF to be typically double the d-axis MMF. To prevent, thus, a high amount of q-axis flux in this region, the widths of the flux barriers in this region (in the middle of the pole) are

increased by the optimisation.

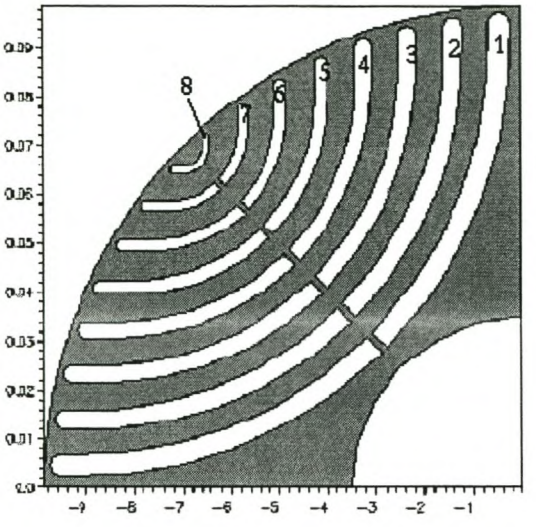

Figure 3.8: Optimised RSM rotor with 64 flux-barriers (16 per pole).

The actual rotor lamination is shown in Figure 3.10. For the prototype rotor the laminations were cut by laser. The lamination steel is of the type 26 ga M19 C5. A laminated core is used to prevent high surface losses in the rotor. The rotor is assembled and is shown in Figure A.2. The performance results of the RSM with this rotor are studied in Chapters 5 and 6.

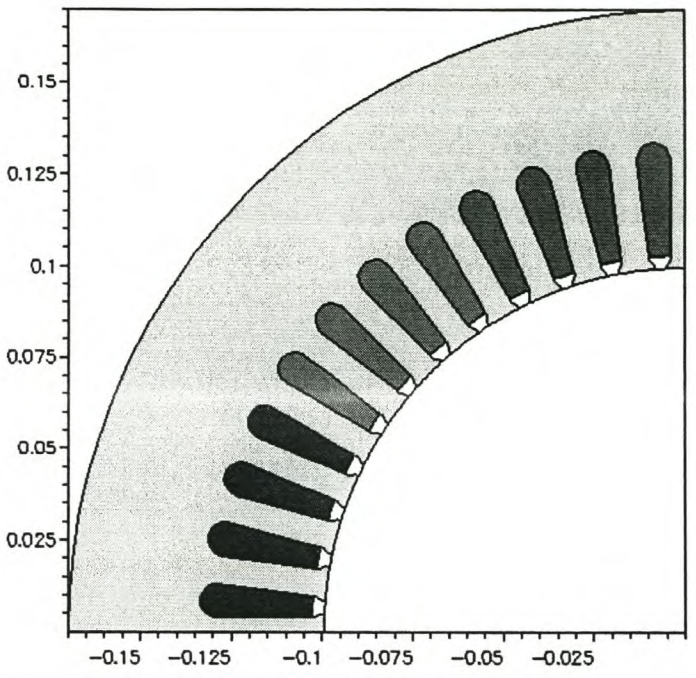

Figure 3.9: Stator used in the optimisation of the rotor.

Figure 3.10: Lamination of a 64-flux barrier RSM rotor

Chapter 4

Effect of Stator Chording and Rotor Skewing

Low torque ripple in electrical machines is generally required to reduce acoustic noise and mechanical resonance vibration. However, to design the electrical machine for low torque ripple, affects the average torque and the power rating of the machine. Consequently, in this chapter the effect of stator winding chording and rotor skewing on the average torque and torque ripple of the normal laminated rotor reluctance synchronous machine is investigated. The effect of barrier position on torque ripple is not investigated in this thesis, as it is, amongst other things, another design method to reduce torque ripple.

Two RSMs are considered in the analysis, namely a small, 36 stator slot machine and a medium power, 48 stator slot machine. Figures 4.1 and 4.2 show the stator and the rotor structures of these two 4-pole, optimum designed, transverse laminated rotor RSMs. The design details and machine dimensions are given in Table 4.1. Both machines have been built and tested under current vector control. The results are published in [1] and [2].

The effect of chording of the stator winding on the torque ripple and average torque is investigated by varying the fractional pitch windings. The effect of rotor skewing is investigated by varying the skew in terms of the number of stator slots.

4.1 Effect of stator chording on torque and torque ripple

Chorded stator windings are used to specifically reduce the lower order 5th and 7th MMF space harmonics. To investigate the effect of chording on the average (fundamental) torque of the RSM,

Table 4.1: Design details of the two RSMs.

	9 kW RSM	42 kW RSM
Parameter	Machine Data	
Stator outer diameter (*mm*)	203	340
Stator inner diameter (*mm*)	105	199
Stack length (*mm*)	133	175
Stack volume (dm^3)	4.3	15.9
Number of poles	4	4
Stator chording	varies	varies
Number of stator slots	36	48
Skew (slot pitches)	varies	varies
Airgap length (*mm*)	0.34	0.62

the torque equation of the machine is considered. The equation is given by

$$T = \frac{3}{2}p(L_{dm} - L_{qm})I_s^2 \sin(2\phi) \ . \tag{4.1}$$

The equations for the d- and q-axis magnetising inductances are given by [5] as follows:

$$L_{dm} = \frac{m(Wk_{w1})^2 d_i l \mu_o}{\pi p^2 g_d k_{sd}} \ , \tag{4.2}$$

$$L_{qm} = \frac{m(Wk_{w1})^2 d_i l \mu_o}{\pi p^2 g_q k_{sq}} \ , \tag{4.3}$$

where m and W are respectively the number of phases and number of turns in series per phase; k_{w1} is the winding factor for the fundamental; d_i is the airgap diameter; l is the core length; p is the number of pole pairs; g_d, g_q are resultant airgap lengths of the d- and q-axis magnetic circuits; k_{sd}, k_{sq} are saturation factors of the d- and q-axis magnetic circuits.

Defining the effective d- and q-axis airgap lengths as

$$g_d' = g_d k_{sd} \tag{4.4}$$

and

$$g_q' = g_q k_{sq}, \tag{4.5}$$

the magnetising inductance difference can be expressed from Equations (4.2) and (4.3) as

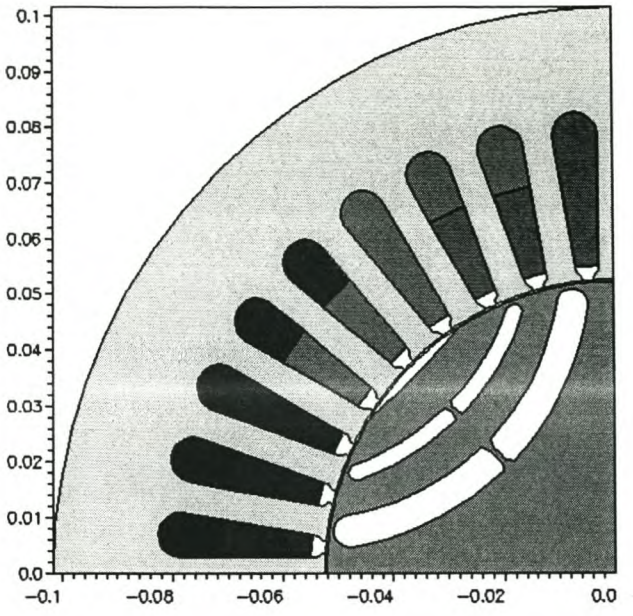

Figure 4.1: One pole segment of RSM stator and rotor with double layer, 8/9 chorded winding (9 kW RSM) [1].

$$\Delta L = L_{dm} - L_{qm} = K_1(k_{w1})^2(\frac{1}{g_d'} - \frac{1}{g_q'}). \tag{4.6}$$

Hence, with constant *rms* current and a constant current angle, the torque Equation (4.1) becomes

$$T = K_2(k_{w1})^2 \left(\frac{1}{g_d'} - \frac{1}{g_q'}\right), \tag{4.7}$$

where

$$K_2 = \frac{3}{2} p K_1 I_s^2 \sin(2\phi). \tag{4.8}$$

Equation (4.7) shows that the torque is a function of the square of the fundamental winding factor. For the nth MMF harmonic, the winding factor is given by [6].

$$k_{wn} = \frac{\sin\left(\frac{n\pi}{2m}\right)}{q \sin\left(\frac{n\pi}{2mq}\right)} * \cos\left(\frac{n\pi}{2}\left(1 - \frac{c}{mq}\right)\right). \tag{4.9}$$

The fundamental, 5th and 7th harmonic winding factors and the estimated change in average torque,

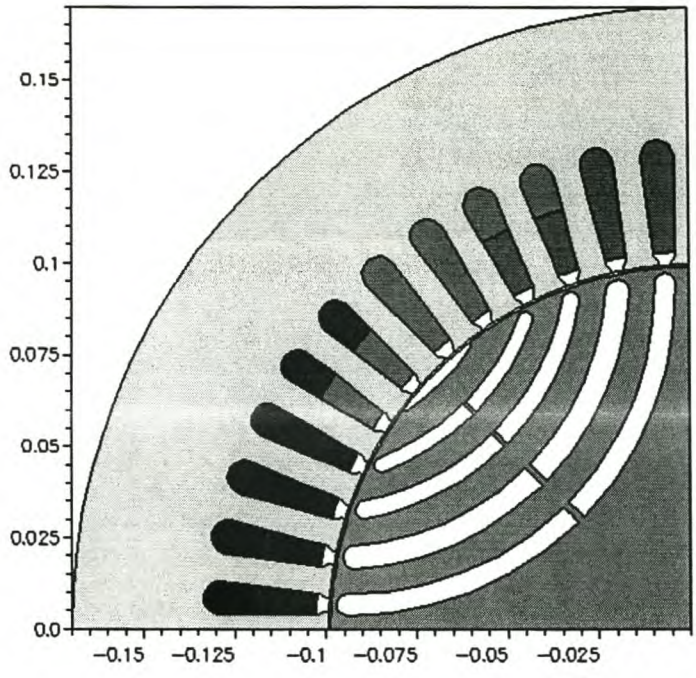

Figure 4.2: One pole segment of RSM stator and rotor with double layer, 10/12 chorded winding (42 kW RSM) [2].

according to Equation (4.7), of the two RSMs considered are calculated and given in Table 4.2. According to these calculations the 7/9-chorded winding for the small RSM and the 10/12-chorded winding for the medium power RSM should be used, if the main focus for chording is to reduce the 5th and 7th MMF harmonics. These conventional chorded windings show to reduce the average torque by 12% and 7%, respectively, according to Table 4.2.

The average torque as a function of winding factor for the two RSMs is also determined from FE analysis. In this analysis the rotor was skewed by, conventional, one stator slot pitch and the current angle was kept constant at a typical optimum angle , namely $\phi = 65^o$ [2] and [3].

The FE calculated results of the average torque versus winding factor are shown in Figures 4.3 and 4.4. These have to be compared with the average per unit torque results of Table 4.2, also shown in Figures 4.3 and 4.4. There is a relative good agreement between the estimated drop in torque (Table 4.2) and the FE calculated drop in torque. At conventional 7/9 and 10/12 chordings, the FE results show that the drop in torque is 8% and 4% for the two machines, respectively. The power ratings, thus, of these two machines drop with these figures, respectively.

The effect of chording on the torque ripple is also determined from the FE analysis. The results are shown in Figures 4.3 and 4.4. Hence, it is clear that the optimum chording for reducing torque

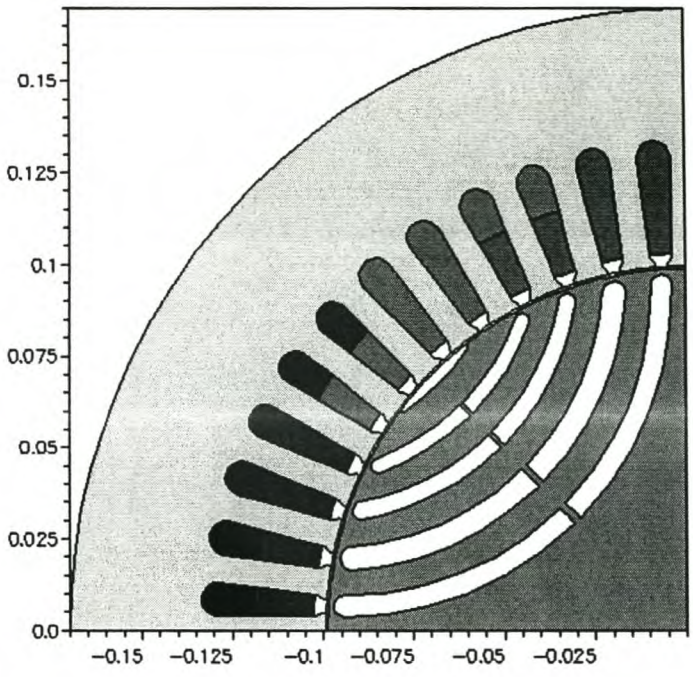

Figure 4.2: One pole segment of RSM stator and rotor with double layer, 10/12 chorded winding (42 kW RSM) [2].

according to Equation (4.7), of the two RSMs considered are calculated and given in Table 4.2. According to these calculations the 7/9-chorded winding for the small RSM and the 10/12-chorded winding for the medium power RSM should be used, if the main focus for chording is to reduce the 5th and 7th MMF harmonics. These conventional chorded windings show to reduce the average torque by 12% and 7%, respectively, according to Table 4.2.

The average torque as a function of winding factor for the two RSMs is also determined from FE analysis. In this analysis the rotor was skewed by, conventional, one stator slot pitch and the current angle was kept constant at a typical optimum angle , namely $\phi = 65^o$ [2] and [3].

The FE calculated results of the average torque versus winding factor are shown in Figures 4.3 and 4.4. These have to be compared with the average per unit torque results of Table 4.2, also shown in Figures 4.3 and 4.4. There is a relative good agreement between the estimated drop in torque (Table 4.2) and the FE calculated drop in torque. At conventional 7/9 and 10/12 chordings, the FE results show that the drop in torque is 8% and 4% for the two machines, respectively. The power ratings, thus, of these two machines drop with these figures, respectively.

The effect of chording on the torque ripple is also determined from the FE analysis. The results are shown in Figures 4.3 and 4.4. Hence, it is clear that the optimum chording for reducing torque

Table 4.2: Calculated winding factors and estimated average torque in per unit.

36 slot RSM (9 kW): k_{wn}				
n	9/9	8/9	7/9	6/9
1	0.96	0.95	0.902	0.831
5	0.2176	0.1399	- 0.0378	- 0.1884
7	- 0.1773	- 0.0607	0.1359	0.1536
T_{avg} (p.u.)	1.0	0.979	0.880	0.749
48 slot RSM (42 kW): k_{wn}				
n	12/12	11/12	10/12	9/12
1	0.958	0.95	0.925	0.885
5	0.2176	0.1726	0.0563	- 0.0833
7	- 0.1774	- 0.1080	0.0459	0.4504
T_{avg} (p.u.)	1.0	0.983	0.932	0.853

ripple does not necessarily coinside with the optimum chording for reducing the 5th and 7th MMF space harmonics. Furthermore, the results show that conventional chording, i.e. 7/9 and 10/12, has no effect on reducing the torque ripple. Finally, the FE calculated torques versus rotor position of the small RSM with different chordings are shown in Figure 4.5, as an example.

4.2 Effect of rotor skewing on average torque and torque ripple

This section investigates the effect of skewing on the average torque and torque ripple of the RSM. Skewing can be represented by using a set of unskewed machines of which the rotors are relatively displaced by an angle that is a fraction of the total skew. This is shown in Figure 4.6(a) where the skewed machine has five submachines. Figure 4.6(b) shows the representation of the unskewed machine with one submachine.

For each submachine the *rms* current is the same, but the current angle and the inductance difference ΔL, differ. Hence, from Equation (4.1), the fundamental torque for each submachine n for a given *rms* current is

$$T_n = K\Delta L_n \sin(2\phi_n), \tag{4.10}$$

where $\phi_n = \phi_1 + (n-1)\alpha$ and α is a skewed angle (Figure 4.6(a)) and ΔL_n is the inductance difference of submachine n. For the skewed machine the average fundamental torque will be

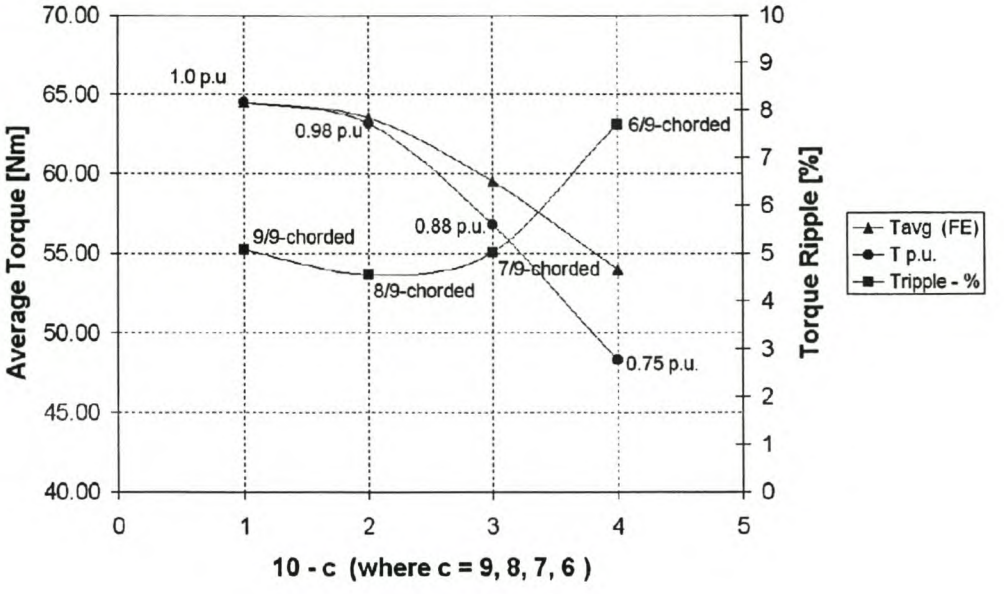

Figure 4.3: Effect of chording on average torque and torque ripple of the small RSM (skew=1 stator slot-pitch; c = coil pitch in terms of number of stator slots).

$$T_{skew} = \frac{1}{k}\sum_{n=1}^{k} T_n, \tag{4.11}$$

where k=5 from Figure 4.6(a). For the unskewed machine the average fundamental torque will be

$$T_{unskew} = T_3 = K\Delta L_3 \sin(2\phi_3). \tag{4.12}$$

The fundamental torque of the RSM as a function of ϕ is already shown and explained by [3] and has a typical shape like that shown in Figure 4.7 at a constant *rms* current. The typical optimum current angle is 65°. Each submachine of Figure 4.6(a) has exactly the same torque versus current angle profile as that shown in Figure 4.7. Running the machine, thus, at a certain average current angle, ϕ_3, the submachine torques, T_n,will be different and it is clear that $T_{skew} < T_3 = T_{unskew}$. The question is how much will the skewed torque be less than the unskewed torque. By considering the torque curve of Figure 4.7 of the 48 stator slot RSM, with the different current angles of the five submachines also shown, it is clear that this difference will be small due to the smooth curve.

To investigate the actual difference between the average torques of the skewed and unskewed RSMs, the FE calculation method is used again for the two machines under consideration. The results of these calculations are shown in Figures 4.8 and 4.9. Skewing the machine by a conventional one

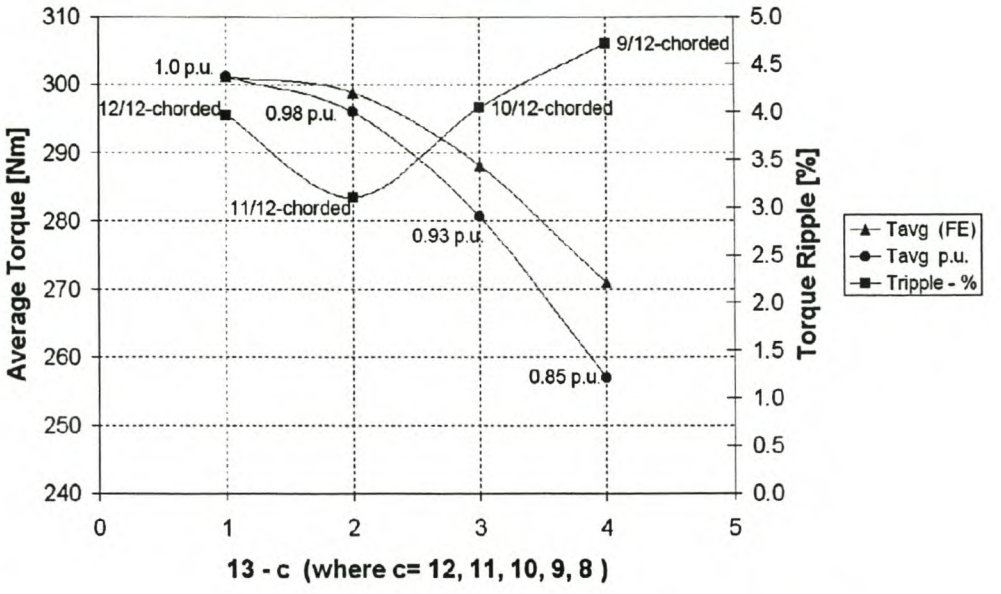

Figure 4.4: Effect of chording on average torque and torque ripple of the medium power RSM (skew = 1 stator slot-pitch; c = coil pitch in terms of number of stator slots).

stator slot pitch causes a drop in average torque of less than 2%, while skewing the machine by two stator slot pitches causes the average torque to drop by 11% for the small RSM and 5% for the medium power RSM. Thus, skewing the rotor by more or less than one stator slot pitch is shown to have negligible drop in average torque for 36 slot and 48 slot RSMs.

The effect of skewing on torque ripple is at the same time determined from the FE analysis and is shown in Figures 4.8 and 4.9. Clearly the torque ripple of both machines is drastically reduced from more than 20% to less than 5%. What is further shown is that the optimum skew is not necessarily at one stator slot pitch. For these two RSMs the optimum skews are at 1.2 and 1.1 stator slot pitches, respectively.

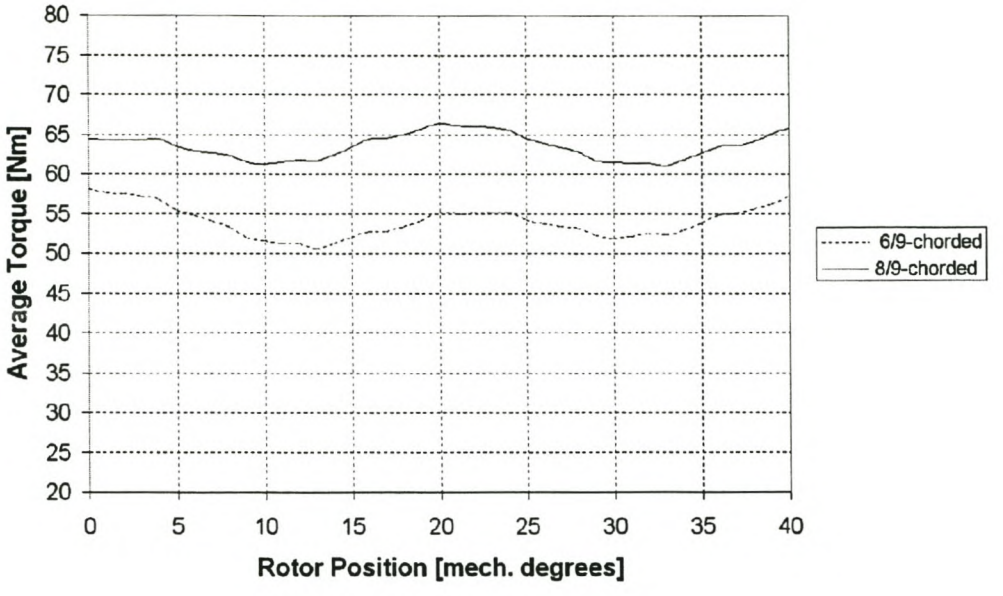

Figure 4.5: FE calculated torque *versus* rotor position of the small, 36 slot RSM ($\phi = 65^0$, skew = 1 stator slot-pitch).

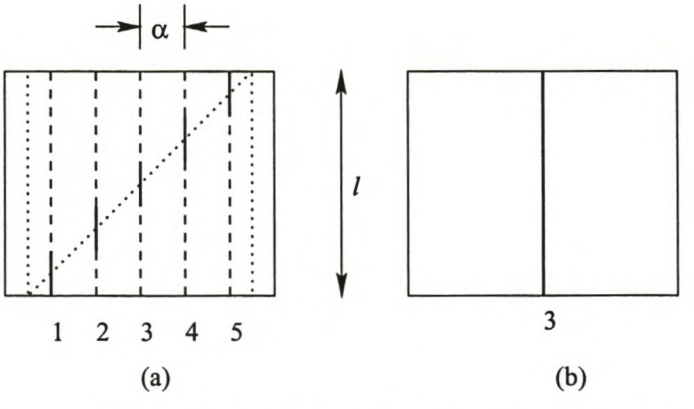

Figure 4.6: Representation of (a) skewed machine with 5 submachines and (b) unskewed machine.

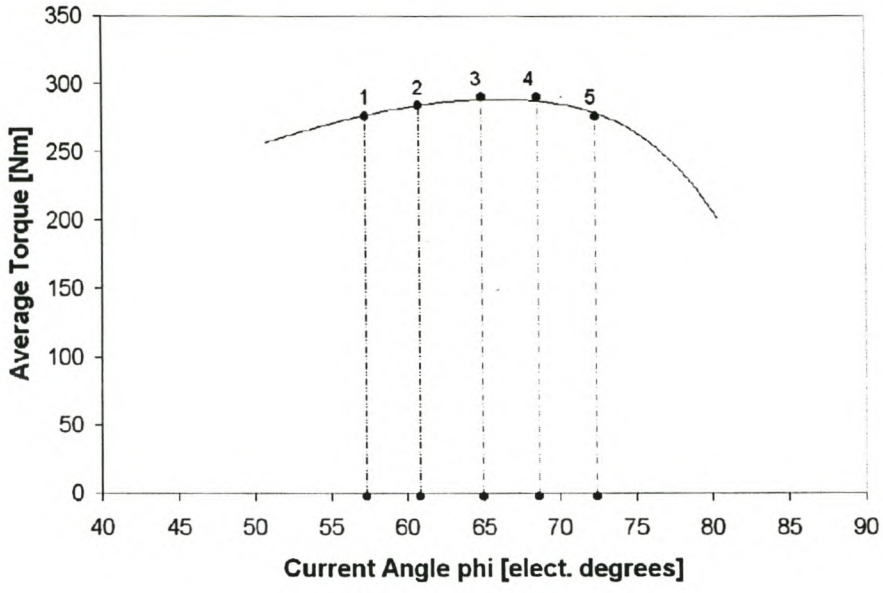

Figure 4.7: Typical torque *versus* current angle curve of the RSM (current angles are shown for 5 submachines skewed one stator slot pitch-conventional skew, with $\phi_3 = 65^0$, of the 48 stator slot RSM).

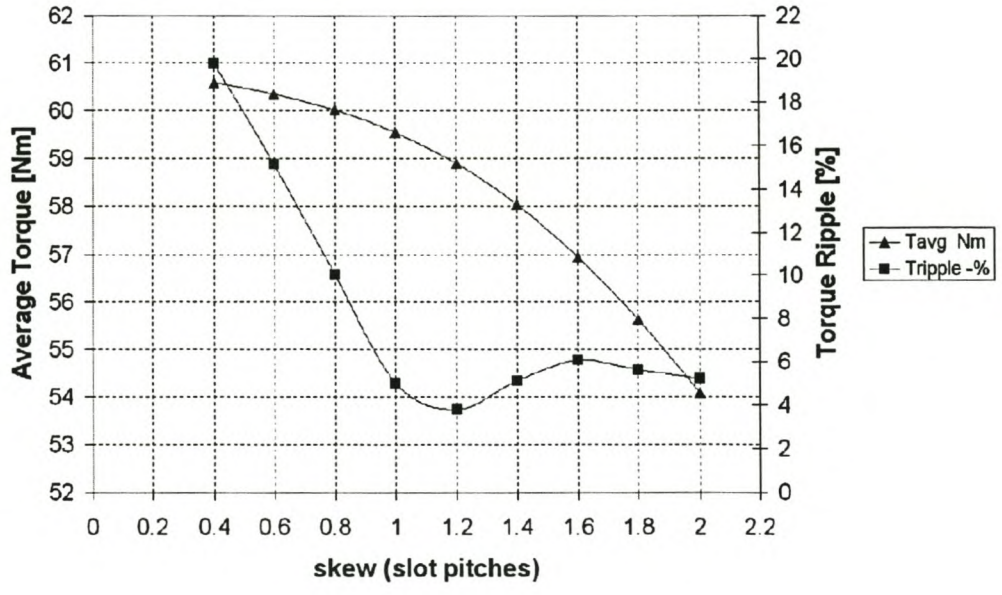

Figure 4.8: Average torque and torque ripple *versus* skew (36 stator slots, small RSM).

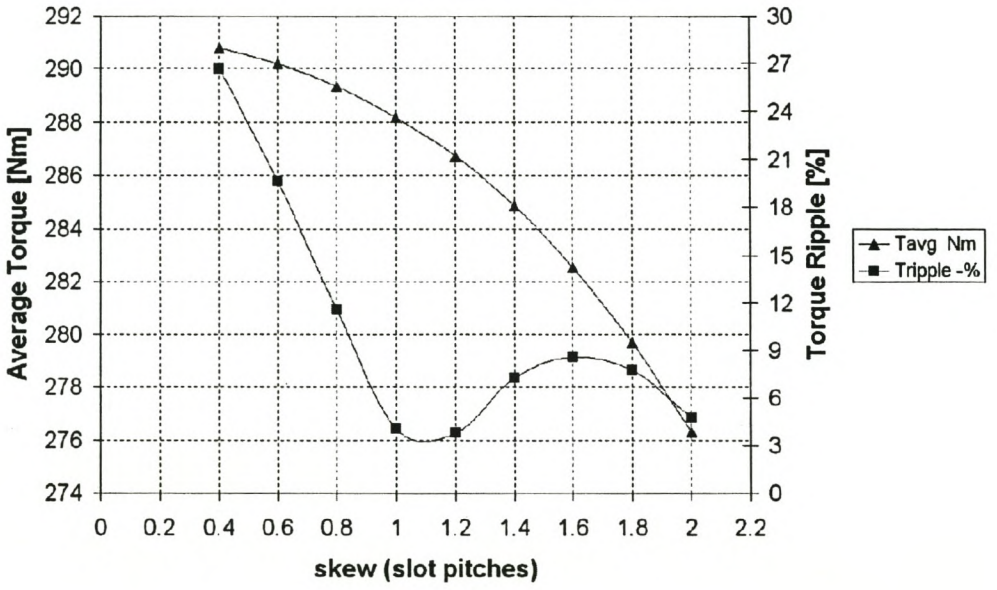

Figure 4.9: Average torque and torque ripple *versus* skew (48 stator slots, medium power RSM).

Chapter 5

Effect of Rotor Flux Barrier to Stator Slot Ratio

The RSM rotor has a number of airgap openings which are called flux-barriers. These are to create magnetic asymmetry on the rotor. There is a limited number of flux-barriers, n_b, per rotor. As a result, certain guidelines in choosing the relevant number of flux barriers per pole is necessary. Firstly, the ratio $\frac{n_b}{p}$, where p is the number of poles, must be an even ratio. Secondly, there is the relation between the number of stator slots, n_{sl}, and the number of flux-barriers per rotor, n_b. To limit iron pulsation losses in the rotor iron segments the barrier pitch in general is taken as larger than the stator tooth pitch, i.e. $n_{sl} > n_b$.

This chapter investigates, to a certain extent, the effect of the $\frac{n_{sl}}{n_b}$ - ratio on the torque ripple and flux pulsations of the RSM. The experimental results of the stator tooth flux pulsations of a medium power reluctance synchronous machine using two different rotors are shown and compared with calculated FE results.

5.1 RSM rotors studied

There are five RSM rotors studied in this investigation. These are shown in Figure 5.1. All the rotors investigated have uniformly distributed flux barriers and the widths of all the flux-barriers in a rotor are taken as the same. The rotors studied are rotors with 32, 40, 48, 56 and 64 flux barriers as shown in Figure 5.1(a) to (e) respectively. The stator is the same in all five cases, with 48 slots and a single layer chorded winding. The airgap of the machine is also not varied.

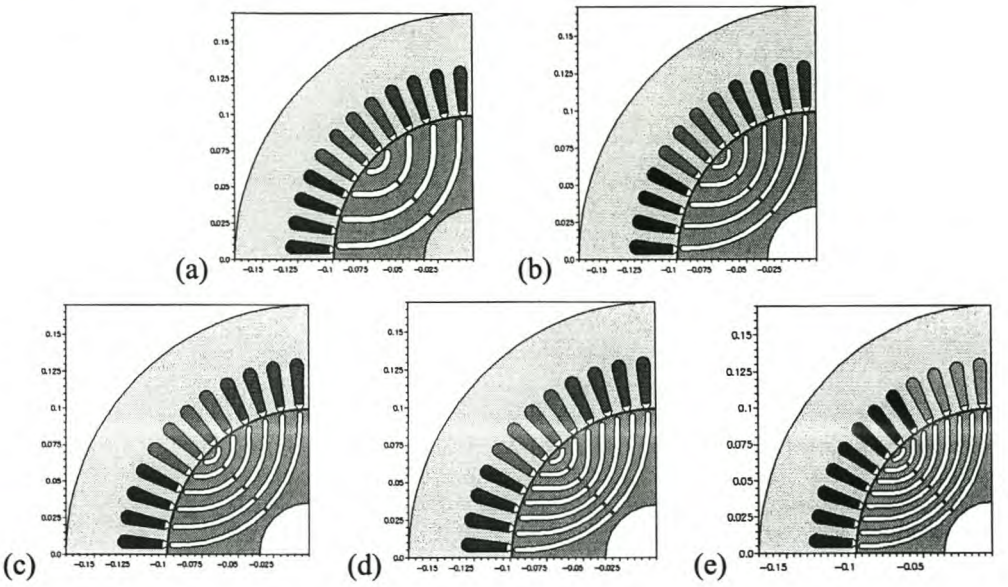

Figure 5.1: Five RSM rotors investigated with a 48-slot, single layer stator.

The ratio of the barrier width, bw, to the barrier pitch, bp, is taken in this analysis as $\frac{bw}{bp} = 0.3$. The immediate question is why? The $\frac{bw}{bp}$ ratio was investigated for axially laminated rotors by both Miller (1991) [10] and Matsuo and Lipo (1994) [12]. They found in general that an optimum ratio of $\frac{bw}{bp} = 0.5$ must be used, which means that the iron segment width must be equal to the barrier width. However, from their results it is clear that the optimum ratio depends on the design criteria considered. The results of Matsuo and Lipo (1993) [11] show that for maximum inductance difference ΔL, which implies maximum torque as expressed by Equation (2.7), the optimum ratio is between 0.26 and 0.33. According to the results of Miller(1991) [10], however, in the case for maximum inductance ratio $\sigma = \frac{L_d}{L_q}$, which implies maximum power factor or maximum torque/kVA , the optimum ratio is about $\frac{bw}{bp} = 0.55$.

The above difference is further explained by Kamper (1996) [5] as follows: Having L_q relatively small, ΔL is most sensitive to the value of the d-axis inductance L_d. To increase L_d and thus ΔL and torque, more iron has to be used on the rotor to make the saturation effect less, that is the ratio $\frac{bw}{bp}$ must be less. On the other hand, the inductance ratio $\sigma = \frac{L_d}{L_q}$ is most sensitive to the value of the q-axis inductance L_q. To decrease L_q, i.e. to increase σ and the power factor and the torque/kVA, larger barrier widths have to be used with thus less iron on the rotor. In this case it means that the $\frac{bw}{bp}$ ratio must be increased. It should be noted that the $\frac{bw}{bp}$ ratio should not be higher than 0.5, because with a peak airgap flux density of say 0.9 *tesla,* the iron segment flux density will then be higher than 1.8 *tesla,* which will drive the rotor iron deep into saturation.

So [5] concludes that it is realistic to choose values for the $\frac{bw}{bp}$ ratio between 0.3 and 0.5. This depends on whether the design optimisation of the RSM is focused on maximising the torque of the machine, of which a ratio of $\frac{bw}{bp} = 0.3$ must be considered, or is focused on maximising the power factor (i.e. maximising the torque/kVA) of which a ratio of $\frac{bw}{bp} = 0.5$ must be used. As said in this study the focus is on maximising torque, so a $\frac{bw}{bp} = 0.3$ is chosen. This can be seen from the rotors in Figure 5.1.

5.2 Effect on average torque and torque ripple

The effect of the flux barriers to stator slot ratio on average torque and torque ripple is illustrated by the FE calculated results of Figure 5.2 on page 37. In the figure the calculated average torque and the torque ripple for each rotor studied are shown. The conclusion drawn out of these results is that $n_b \neq n_{sl}$. For example, if we have $n_b = n_{sl} = 48$, an extraordinary high torque ripple is noticed from Figure 5.2, which is caused by cogging torques. As a result, Equation (5.1) gives how many flux barriers can be used in a RSM rotor with the number of stator slots taken into account:

$$n_b = p * k \,, \tag{5.1}$$

where p = number of poles, $k = 2, 4, 6, 8, \ldots$ and $k \neq \frac{n_{sl}}{p}$. In this thesis $p = 4$, i.e. all the RSMs studied are 4-pole machines. As it was mentioned earlier that $\frac{n_b}{p}$ must be even, the cases considered in this research are where $\frac{n_b}{p} = 8, 10, 12, 14, 16$. A further result noticed from Figure 5.2 is that the torque ripple is lower with $n_b > n_{sl}$. For example, with the 64-flux barrier rotor ($\frac{n_b}{p} = 16$) the torque ripple is almost 50% less than that with the 32-flux barrier rotor with no compromise of whatsoever in average torque. The average torque for all five rotors are very much the same.

5.3 Flux pulsations in stator teeth and rotor iron

High frequency flux pulsations increase the stray load losses and decrease the efficiency of electrical machines. These high frequency flux pulsations can occur in the stator teeth and rotor iron segments of the reluctance synchronous machine, depending on the rotor design. It is shown in this section how flux pulsations depend on the ratio of the stator slots to the number of rotor inner flux barriers used. FE analysis is used to study the occurrence of flux pulsations in the machine. The author, however, proposes a further detail study in this field.

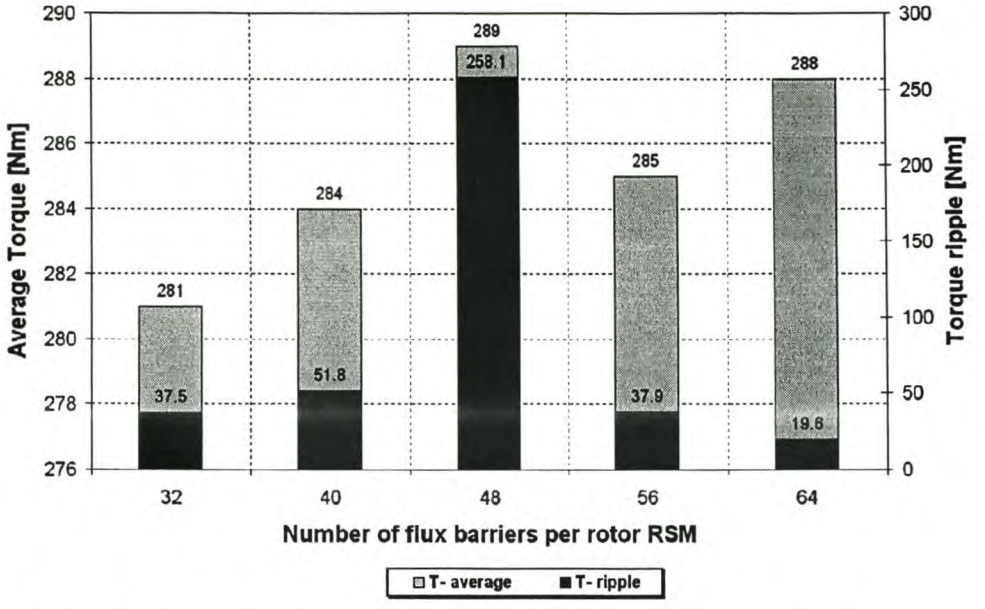

Figure 5.2: 37Average torque and torque ripple of the 32, 40, 48, 56 and 64 flux barrier rotor RSMs (rotors are unskewed).

Flux pulsations in the stator and rotor teeth of induction machines (IM) is a well-known phenomenon. Some available literature on the latter is in [19]-[23]. Due to the slotted airgap of the machine and the relative motion between the stator and rotor teeth, flux pulsations occur which deeply penetrate the stator and the rotor teeth. These flux pulsations lead to additional iron losses in the teeth of the machine and are called tooth pulsation losses. These losses can have a considerable negative effect on the efficiency of the machine.

In Figure 5.3(a) a conventional, two-pole, low performance rotor reluctance synchronous machine (RSM) is shown. The rotor shown has two cut-outs on the sides acting as flux barriers. The stator is conventional, as it is the stator for the IM as well. This machine, in contrast with the IM, has no high frequency tooth pulsation losses as the rotor is not slotted. However, in the case where the RSM has no cut-outs but a relatively high number of inner flux barrier openings, such as that shown in Figure 5.3(b), tooth pulsations again will occur. In the latter case the situation of the tooth pulsation losses is more severe than in the case of the IM as the rotor teeth consists of long iron segments. If high frequency flux pulsations occur along these rotor iron segments, the tooth pulsation losses in RSMs using these type of rotors will be high and the efficiency consequently low.

The additional tooth pulsation losses that occur in RSMs that use axially laminated rotors have been reported in literature [18], [19]. Axially laminated rotors has a high number of inner flux barriers which are open at the surface of the rotor, i.e. the rotor has a highly slotted pole surface. This will

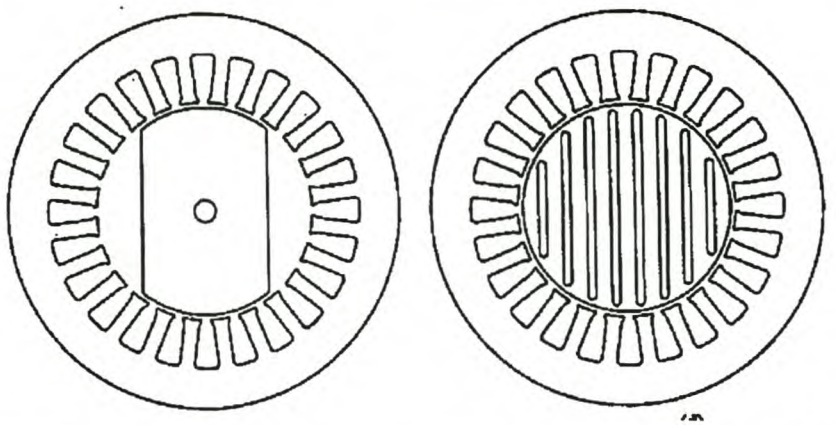

(a) (b)

Figure 5.3: Cross section of (a) Conventional RSM, (b) RSM with inner flux barrier rotor.

give rise to high tooth pulsation losses in the rotor which amongst other things will raise the rotor temperature. Some ways had been followed to lessen the tooth pulsation losses namely (i) to operate the machine at a lower magnetisation level, (ii) to use less inner flux barriers in the rotor and (iii) to ensure in the rotor design that the iron segments are properly placed with respect to the stator teeth and slots, i.e. if one end of a rotor iron segment is against a stator tooth, then the other end must be against a stator slot [19].

The question is to what extent do flux pulsations and tooth pulsation losses occur in RSMs that use inner flux barriers in the rotor which are closed at the rotor surface. With closed inner flux barrier rotors, one might expect that the flux pulsations will be much less and that a higher number of flux barriers can be used. As this section investigates the flux pulsations that occur in the stator teeth and rotor iron segments of the RSMs that use rotors with closed inner flux barrier openings, the effect of the stator and rotor design on these flux pulsations is shown and conclusions on the design are reached.

5.3.1 Calculation of flux pulsations

The flux pulsations in the stator teeth and rotor iron segments of the RSM are calculated through FE analysis and by stepping the rotor in the FE analysis through a certain angle to observe the flux density variation. To explain the calculation of the flux pulsations, consider the typical stator and rotor structure of a 4-pole RSM shown in Figure 5.4.

The flux density variation is calculated at four positions in the machine. These four positions are shown in Figure 5.4. Two calculation points are in a rotor iron segment (one close to the surface and one deep in the iron segment) and two in a stator tooth (one near to the airgap and the other

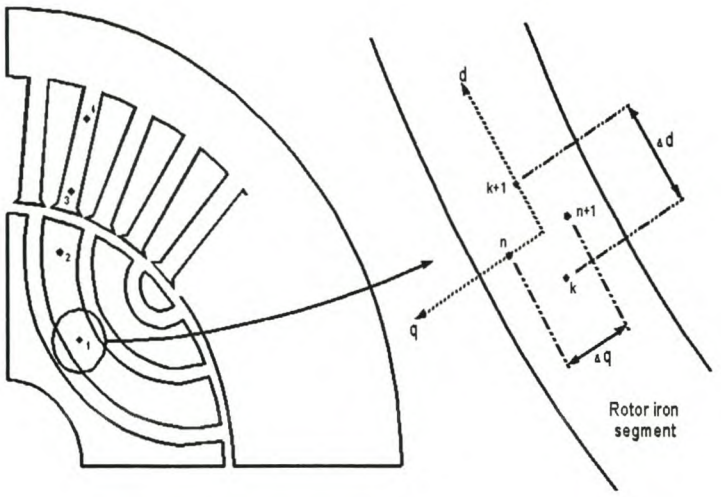

Figure 5.4: RSM structure and flux density calculation points

deep in the stator tooth). In the rotor iron segment the flux density variation is calculated in two directions namely: the one aligned with the iron segment (d-direction) and the other perpendicular or in quadrature to the iron segment (q-direction). In the stator tooth the flux density variation was only calculated in the d-direction.

To calculate the fundamental flux density on the rotor iron segment, the flux density vector can be expressed in terms of dq- plane as explained in [5].

$$\hat{B} = \frac{\partial A_z}{\partial q} u_d + \left(-\frac{\partial A_z}{\partial d} \right) u_q \tag{5.2}$$

where u_d is the unit vector directed in the d-direction, and u_q is the unit vector that points in the direction of increasing q-axis. The partial derivatives of A_z with respect to the d and q directions can be determined by the finite difference approximation as expressed in Equations (5.3) and (5.4) below. These two general equations are for calculating the flux densities using 2-D finite element analysis and are as follows (see Figure 5.4):

$$B_d = \frac{A_{z(n+1)} - A_{z(n)}}{\Delta q}, \tag{5.3}$$

$$B_q = \frac{A_{z(k+1)} - A_{z(k)}}{\Delta d}. \tag{5.4}$$

A_z is the magnetic vector potential in the z-direction. Equations (5.3) and (5.4) are used to calculate four d-axis flux densities (B_{d1-4}) at the four positions in the machine and two q-axis flux densities in the rotor segment (B_{q1-2}).

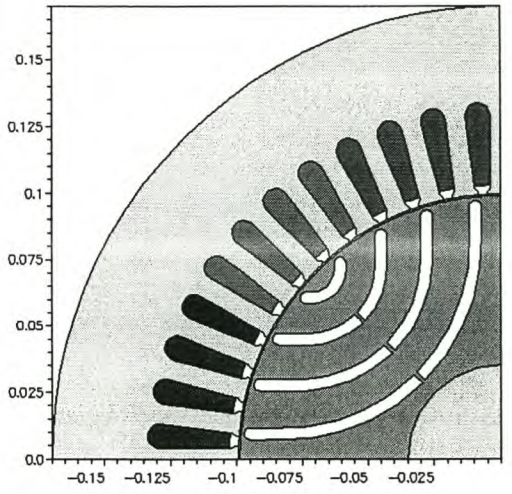

Figure 5.5: RSM 4-pole structure with 32 rotor flux barriers.

5.3.2 Calculated and measured results

The 4-pole, 48-slot stator RSM was used with flux barrier rotors of different designs, for the calculated and measured results. These flux barrier rotor designs were different in (i) number of flux barriers used, (ii) width of the flux barrier and (iii) height of the iron rib (at the surface of the rotor). The stator differs only in (i) semiclosed slots and (ii) open slots. An example of a RSM structure analysed in the FE analysis is shown in Figure 5.5.

In Figure 5.6 the flux density in the upper rotor iron segment, B_{d2}, is shown, for example, for the standard RSM with different number of flux barriers used on the rotor. The standard machine is the RSM with normal nonzero rib heights, stator with semiclosed slots (normal) and the barrier widths of according to $\frac{bw}{bp} = 0.3$ ratio. Figure 5.7 shows a summary of the flux density variation, ΔB_{d2}, versus the number of flux barriers for (i) the standard (std) machine, (ii) the rotor with zero rib height (*rh=0*), (iii) the rotor with a barrier width to barrier pitch ratio of $\frac{bw}{bp} = 0.5$ and (iv) the stator with open slots. In the worst cases the zero rib heights increase the flux pulsations in the machine by 17% while the open stator slots increase the flux pulsations by almost 50%. This shows that the combination of zero rib heights and the open stator slots would increase the flux pulsations of the machine significantly, compared to the standard machine. Figures 5.8 and 5.10 show the stator tooth

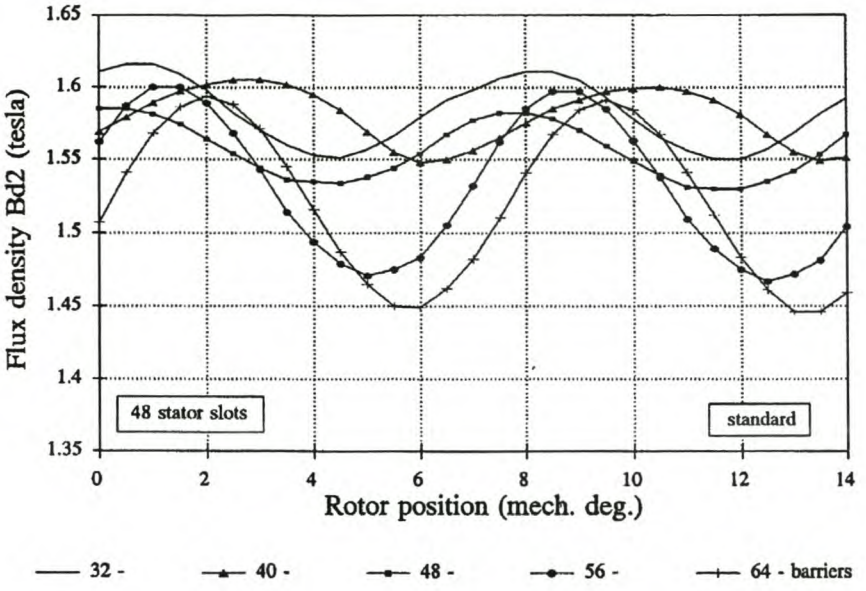

Figure 5.6: Rotor iron flux density Bd2 for the standard RSM rotors

flux density, B_{d3}, for the standard machine using a rotor with 32 and a rotor with 64 flux barriers respectively.

To verify the calculated results to some extent, the stator tooth flux pulsations of a RSM with two different rotors have been measured by means of a test coil around one stator tooth and an electronic circuit that integrates the measured induced voltages. The electronic circuit is shown in Figure 5.12. The circuit has three parts: the first part is a high impedance RC-intergrator, the second part is a voltage buffer with amplifier and the last part is a low-pass filter with a cut-off frequency of 10 kHz. An HP oscilloscope was used to capture the output measured waveforms shown in Figures 5.9 and 5.11. The measured waveforms are obtained with the RSM at full-load at a speed of 100 *rpm*. These results have to be compared with the results of Figures 5.8 and 5.10, although the rotors used in the calculations and the actual rotors are not precisely the same. The actual 32-flux barrier rotor has cut-outs as shown in Figure 1.1(c), while the actual 64-flux barrier rotor has uneven flux barrier widths with no cut-outs as shown in Figure 3.10. Nevertheless, with the slight difference in these rotors the agreement between the measured and the calculated results can be observed.

5.3.3 Discussion of results

The flux density in a stator tooth using a 32-flux barrier rotor has a high ripple (Figure 5.8) as compared to the flux density in a stator tooth when using a 64-flux barrier rotor (Figure 5.10). In

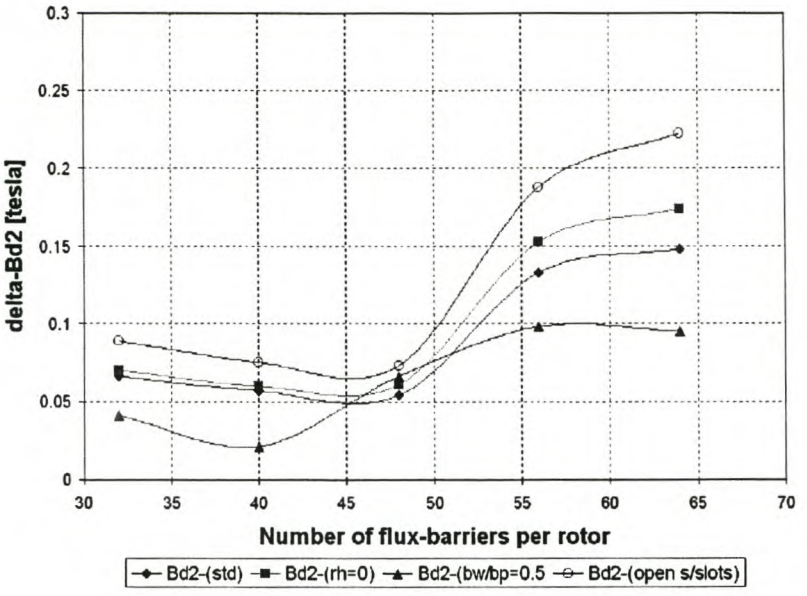

Figure 5.7: Rotor iron flux density variation delta-Bd2

fact with the 64-flux barrier rotor the stator tooth flux density is very smooth and shows about no ripple. The reason for the difference in the tooth flux pulsations is that when using a rotor with a high number of flux barriers, or else a RSM with a high $\frac{n_b}{n_{sl}}$ - ratio rotor, the stator "sees" little variation or change in rotor iron as the rotor rotates. The opposite is true when using a rotor with a low number of flux barriers, or a RSM with a low $\frac{n_b}{n_{sl}}$ - ratio rotor. This smoothness in the flux density results in a low torque ripple. Figure 5.2 confirms that the RSM with the 64-flux barrier rotor has a low torque ripple.

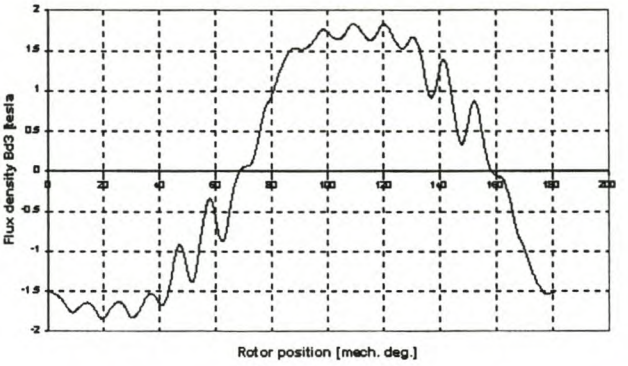

Figure 5.8: Calculated flux density in stator tooth with a 32- flux barrier rotor

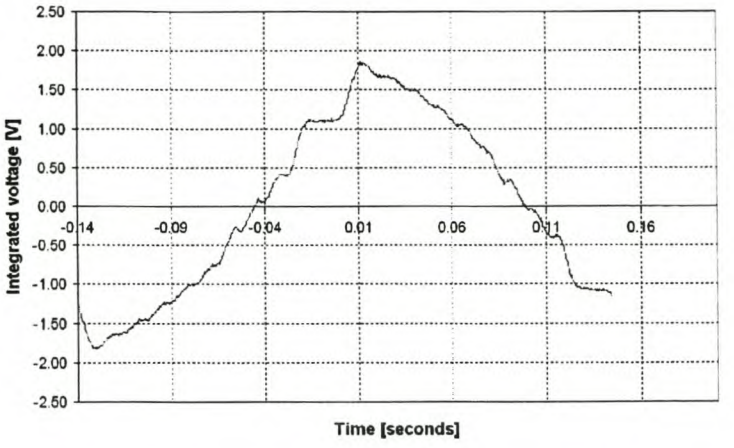

Figure 5.9: Measured stator tooth flux waveforms with nearby 32-flux barrier rotor at low speed.

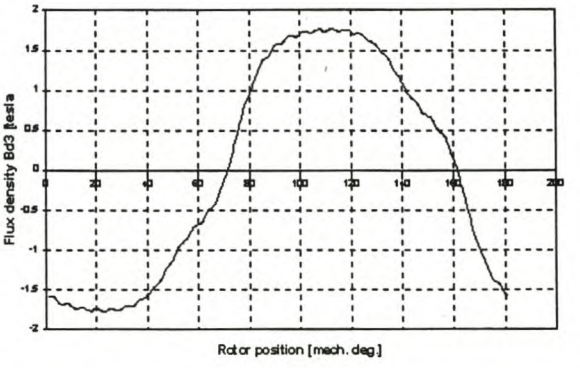

Figure 5.10: Calculated flux density in stator tooth with a 64-flux barrier rotor

5.4 Summary of findings

In general, the flux pulsations are relatively low in the rotor iron segments but relatively high in the stator teeth if the number of flux barriers is less than the number of stator slots. The opposite is true if the number of flux barriers are higher than the number of stator slots, which results in a torque with a low ripple. In the latter case it is found and shown that the rotor iron flux pulsations are double that when using a lower number of flux barrier rotor.

At rated current it is found that the flux pulsations in the deeper rotor iron is about 30% less than the flux pulsations more close to the airgap. This gives an indication of how deep the flux pulsations penetrate into the rotor iron segments. With regard to the stator teeth it is found that the flux pulsations in the lower and deeper stator tooth are almost the same.

Finally, it is found that zero rib heights on the rotor slightly increase the flux pulsations in the rotor,

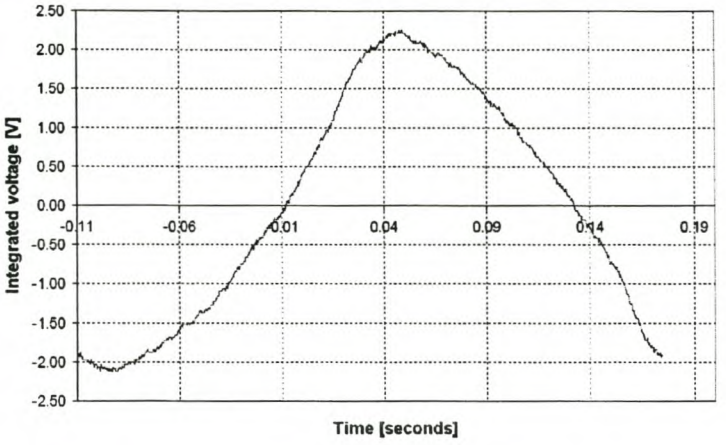

Figure 5.11: Measured stator tooth flux waveforms with 64-flux barrier rotor.

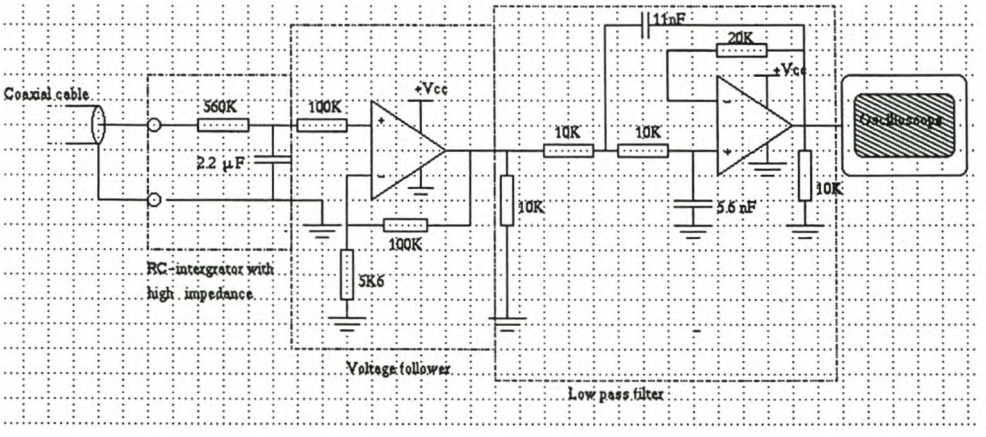

Figure 5.12: Electronic circuit that intergrates the measured induced voltage

while the open stator slots increase the rotor flux pulsations significantly.

Chapter 6

Calculated and Measured Results

In order to verify the accuracy of the FE analysis, measurements need to be performed on different designed RSMs. This chapter discusses the calculated and measured results of the three RSMs studied namely:

Machine 1: chorded and skewed, 32 flux-barrier rotor RSM;

Machine 2: single layer, unskewed, 32 flux-barrier rotor RSM and

Machine 3: single layer, unskewed, 64 flux-barrier rotor RSM.

6.1 Test system

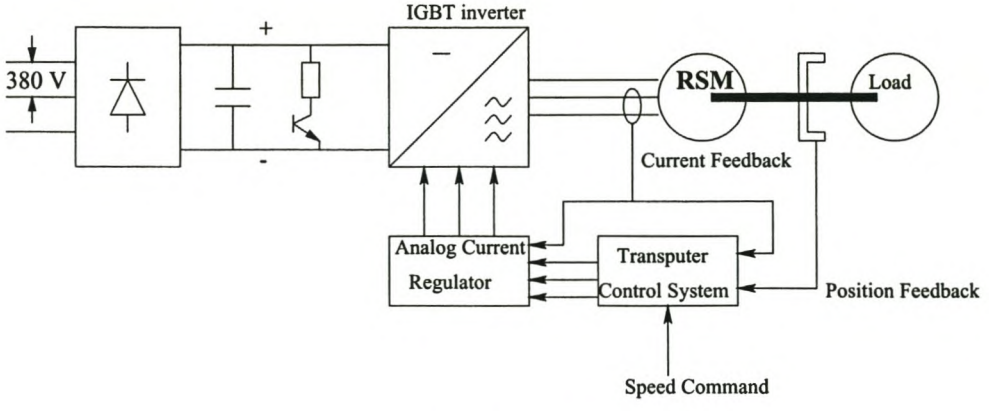

Figure 6.1: The RSM drive system

A block diagram of the RSM drive system is shown in Figure 6.1. It consists of four basic components namely the RSM, the rectifier and inverter, the control system and the load. The power

electronic converter consists of a three-phase diode rectifier, an IGBT three-phase inverter, a large bank of capacitors and a regenerative brake. The highest DC voltage possible is 540 V, rectified from the 380 V AC available in the laboratory. The phases of the RSM are isolated and controlled separately by means of three independent full bridge IGBT converters. The RSM is controlled by a T800 Transputer system with current and position feedback as shown in Figure 6.1. An analog current regulator is used to regulate the AC current in the machine according to the command signals given by the transputer. For the position feedback a small resolver is used which is mounted at the non-drive end of the RSM. Together with the resolver a R-D converter chip is used to obtain a 12-bit digital position signal and also an analog speed signal. Two high speed eddy current dynamometers as load are installed in the laboratory for testing the RSM drive. The dynamometers can be used at speeds up to 10000 *rpm* and torques up 400 Nm each, i.e. 800 Nm in total. A torque transducer is included in each dynamometer for the measurements of the torque.

6.2 Machine 1: Results of chorded and skewed RSM

The RSM under consideration in this section is a forced air-cooled machine with 48 stator slots with chorded winding (10/12-pitch winding), and with a rotor skewed by one-stator slot pitch. This RSM is designed for a wheel drive for a diesel-electric vehicle [15]. The rotor structure for this RSM is shown in Figure 4.2 of Chapter 4.

A short time duration peak torque of 640 Nm (2.3 p.u.) at low speeds and a maximum speed of 6000 *rpm* were required for this machine. The machine is optimum designed with a FE optimisation procedure by maximising the torque at 2.3 times full-load current. Finite element mechanical strength analysis was used for the mechanical design of the rotor at maximum speed with web widths and rib heights taken into consideration. The rated power and torque of the machine are 42 kW at 1500 *rpm* and 267 Nm, respectively. The current controlled drive system of Figure 6.1 is used for the test of this medium power RSM. A 200 kVA inverter operating from an 800 V d.c. bus is developed to supply the machine. For the measurement of the torque and for the load of the machine the two dynamometers mentioned in section 6.1 above are used.

The steady-state performance tests on this machine are conducted at rated speed, which is 1500 *rpm*, and at loads up to two times the full load. The measured and FE calculated torques versus current angle ϕ_1 of the machine at 1500 *rpm* are illustrated in Figure 6.2, with the per unit phase current I_s as a parameter.

Good correlation between calculated and measured results are obtained for currents and torques up to 2.0 p.u. current and torque. It is shown that the optimum current angle increases with load, but

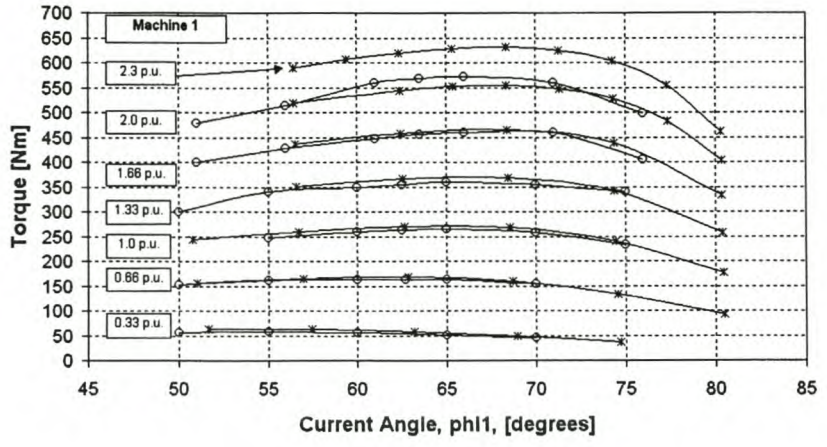

Figure 6.2: Machine 1: Torque *versus* current angle with current I_s in $p.u.$ as a parameter, ($*-$calculated, $o-$ measured).

there is little difference in torque if the angle is kept constant for all loads at a value of say 68^0.

In Figure 6.3, the relation between torque and *rms* phase current is shown for an optimum current angle of 68^0. The interesting result shown in this figure is the almost linear relationship between torque and *rms* phase current. There is a slight flattening at higher loads, over 500 Nm and 200 A *rms* phase current. Theoretically and according to the Equation (2.7) on page 10 of Chapter 2, the relation between torque and *rms* phase current is quadratic. This is in contrast with the calculated and measured relations as it is more linear. The linearity in the torque and *rms* phase current relation is due to saturation and cross-magnetisation which affects ΔL in Equation (2.7). These effects are taken into account by the FE analysis.

In Figure 6.4, the FE calculated efficiency and power factor of machine 1 at 1.0 $p.u.$ current are shown. A maximum efficiency of 92.4% is calculated at an optimum current angle of 68^0. The maximum power factor of 0.76 is at a current angle of 73^0.

Temperature rise measurements of the stator winding of this medium power RSM were also conducted. The change of the stator resistance with temperature was used to determine the temperature change of the stator winding. At continuous full-load (42 kW @1500 *rpm*) the temperature rise, ΔT, is measured as 60^0C. At 2.0 $p.u.$ torque and current and 1500 rpm (i.e. 87 kW) the machine was run for 3-minutes, and the measured temperature rise was 110^0C. It must be mentioned again that forced air cooling was used for this machine.

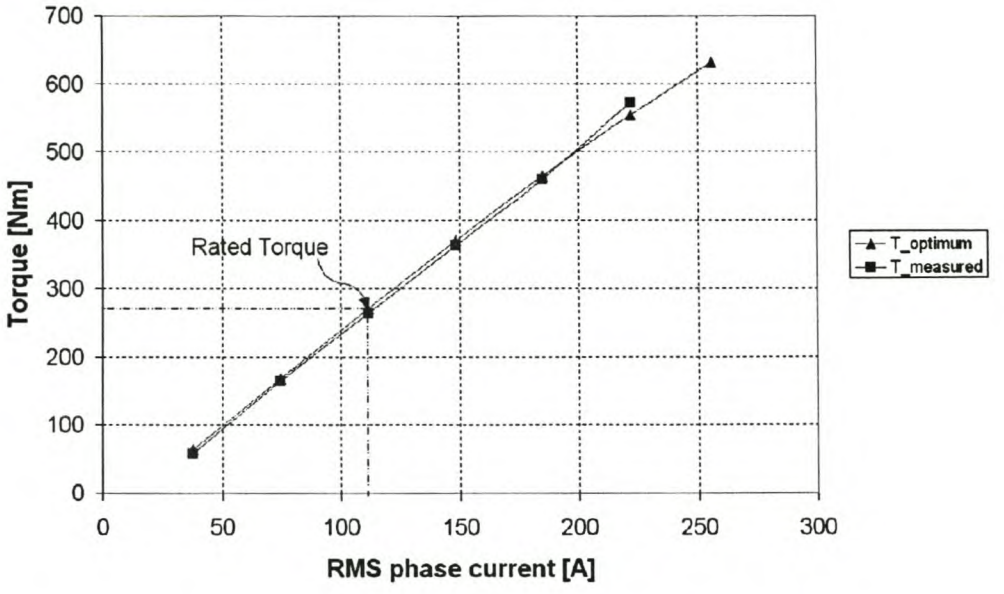

Figure 6.3: Machine 1: Torque *versus rms* phase current (optimum $\phi_1 = 68^0$).

6.3 Machine 2: Results of the single layer unskewed RSM

The RSM under consideration in this section is the same as the one in section 6.2, but with the rotor unskewed and the stator with a single layer winding. The calculated and measured results of average torque of the machine versus the current angle ϕ_1 are shown in Figure 6.5. The FE calculations are up to 2.3 p.u. current, while the measurements are only up to 1.33 p.u. current as the comparison between the machines is round about rated current. Note that there is a relatively good correlation between the measured and the calculated torques of the machine. The torque versus current relationship of the single layer unskewed machine 2 is the same as that of the double layer skewed machine 1, accept that the torque is higher of machine 2. From the FE calculations there is an improvement of about 10% of calculated torque (see Figures 6.2 and 6.5). However, the torque ripple is higher in machine 2 than in machine 1 as is shown by the FE calculations of Chapter 4.

The FE calculated results of efficiency and power factor of the machine 2 are shown in Figure 6.6. At 1.0 p.u. current and optimum current angle of 68^0, this machine has a maximum efficiency of 92.7%. The maximum power factor of the machine is 0.77 at a current angle of 74^0.

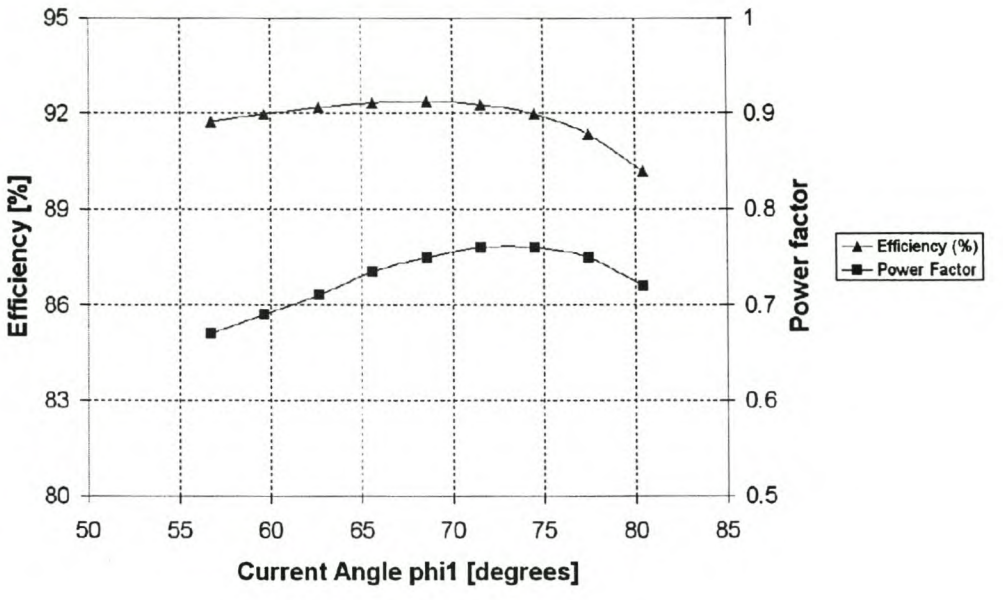

Figure 6.4: Machine 1: Calculated efficiency and power factor *versus* current angle at 1.0 *p.u.* current.

6.4 Machine 3: Results of the 64-flux barrier rotor RSM

The rotor structure for the 64-flux barrier rotor RSM is shown in Figure 3.10. It is an unskewed rotor. The stator used is still the same stator with 48 slots and an unchorded single layer winding. The calculated and measured results of this machine is shown in Figure 6.7. The torque of this machine is the same as that of machine 2, and thus has also a higher average torque than machine 1 as is shown in Figure 5.2 of Chapter 5. In contrast with the other two RSMs discussed in sections 6.2 and 6.3, this machine has a significantly lower torque ripple. From Figure 6.7 it is observed that there is a good agreement between the calculated and measured torques. Once more it must be mentioned that the measured results were carried out up to 1.33 p.u. as the focus of comparison is round about rated current.

Figure 6.8 shows the FE calculated efficiency and power factor of machine 3. The efficiency and power factor are at maximum values at current angles of 68^0 and 75^0 respectively. The overall comparison of the results of the machines discussed above is further discussed in section 6.5.

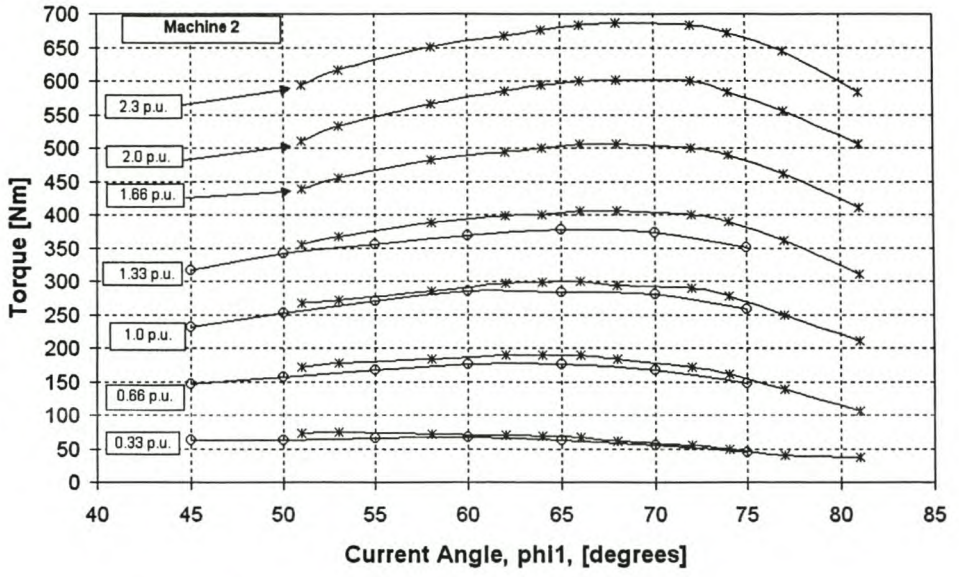

Figure 6.5: Machine 2: Calculated and measured torque *versus* current angle ϕ_1, for the single layer unskewed RSM ($*-$calculated, $o-$ measured).

6.5 Comparison of the three RSMs

This section compares the three RSMs in terms of average torque, efficiency and power factor. The three RSMs are machines 1, 2 and 3 as discussed above. Table 6.1 and Figure 6.9 summarise the results of sections 6.2, 6.3 and 6.4. The values given for efficiency and power factor are FE calculated values. It must be noted that high flux pulsation iron losses in the rotor are not included in the calculated results of Figure 6.9, which give an unfair advantage to machine 3 specifically with regard to efficiency.

It is concluded from the results of Table 6.1 that the performance of the three machines are overall the same, except the higher output torques of machines 2 and 3.

Table 6.1: Comparison of RSMs on Torque, Efficiency and Power factor.

(at 1 p.u. current, $\phi_1 = 68^0$)	Machine 1	Machine 2	Machine 3
Torque T, (measured in [Nm])	267	285	280
Efficiency η, [%]	92.40	92.7	92.9
Power Factor, pf	0.76	0.77	0.76

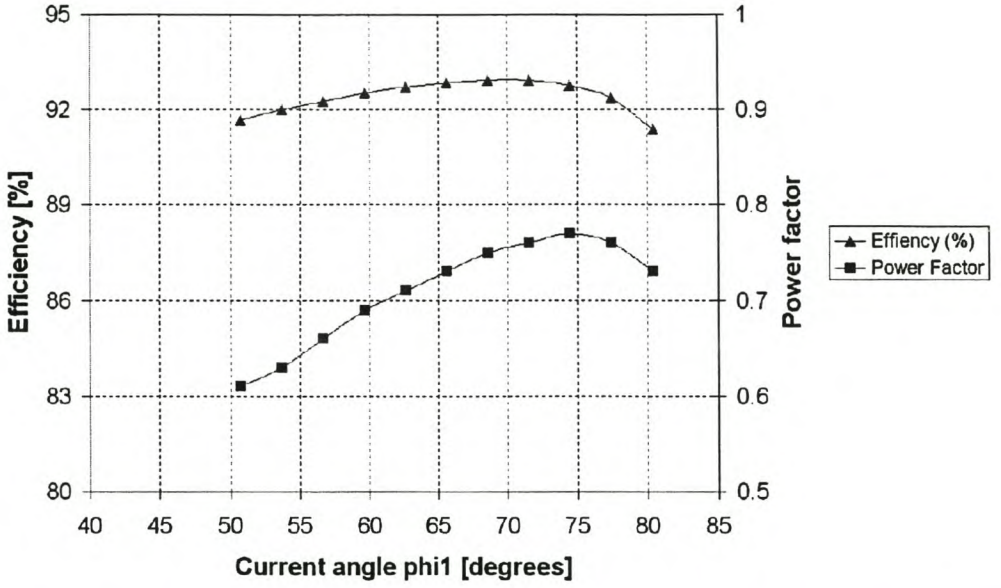

Figure 6.6: Machine 2: Calculated efficiency and power factor *versus* current angle at 1.0 p.u. current for the single layer unskewed RSM

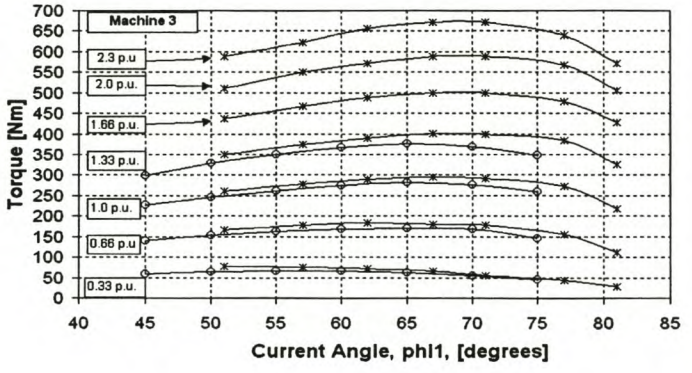

Figure 6.7: Machine 3: Calculated and measured torque *versus* current angle ϕ_1, for the 64-flux barrier rotor RSM ($*-$calculated, $o-$ measured).

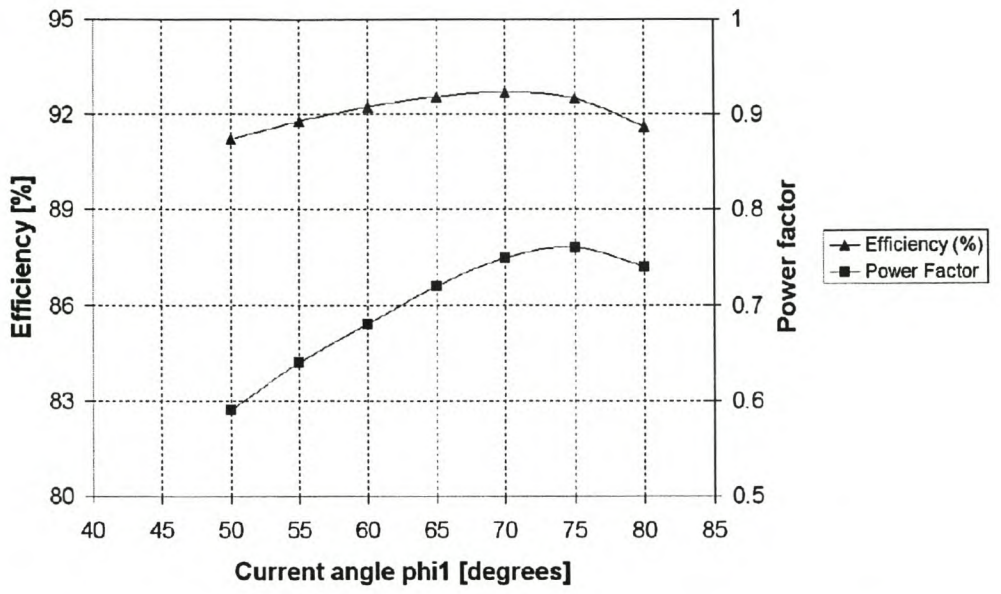

Figure 6.8: Machine 3: Calculated efficiency and power factor *versus* ϕ_1, at 1.0 p.u. current for the single layer unskewed RSM with the 64-flux barrier rotor.

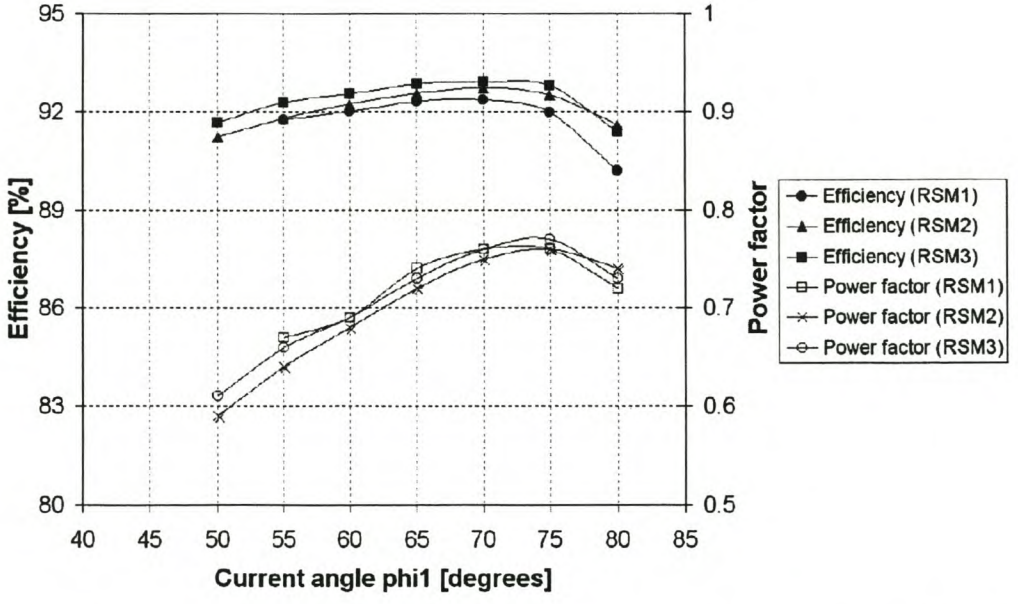

Figure 6.9: Calculated efficiency and power factors versus current angle ϕ_1 for the three RSMs.

Chapter 7

Conclusions and Recommendations

In this thesis some of the design aspects of the multi-flux barrier rotor RSM is studied using 2-D finite element analysis. With the FE analysis the effects of saturation, cross-magnetisation and skew on the performance of the RSM are taken into account. Also the FE analysis is used in an optimisation procedure to optimise the design of the rotor of the RSM. In the following sections the conclusions are summarised of the effects of the different designs on the performance of the RSM. In section 7.4 the recommendations are given.

7.1 Effect of stator chording and rotor skewing

Chording is shown to have a significant effect on average torque and the power rating of the machine. On the basis of reducing the 5^{th} and 7^{th} MMF space harmonics, chording is shown in general to have little effect on the torque ripple. The general conclusion, thus, is that chording is not necessary for the RSM.

Skewing the rotor by the conventional one stator slot pitch shows to have little effect on the developed torque of 36- and 48-stator slot RSMs. For lower number of stator slots the effect of skewing the rotor by one stator slot pitch is shown to be more significant. It is also found that skewing the rotor by one stator slot pitch reduces the torque ripple drastically. However, skewing by one stator slot pitch is shown not to be necessarily the optimum in reducing the torque ripple of the RSM. In general, thus, it is concluded that the RSM-rotor must be skewed by one stator slot pitch.

7.2 Effect of number of rotor flux-barriers

It is found that the flux pulsations are relatively low in the rotor iron segments but relatively high in the stator teeth of the RSM if the number of flux barriers is less than the number of stator slots. The opposite is true if the number of flux barriers are higher than the number of stator slots. In this case it is found and shown that the rotor iron flux pulsations are double that when using a lower number of flux barrier rotor. With the higher number of flux barrier rotor the torque ripple is also found to be low.

It is difficult to come to a general conclusion on the flux-barrier to stator-slot ratio that must be used for RSMs in their designs. Maybe it is better to keep the number of flux barriers less than the number of stator slots, specifically if open stator slots are used, but this must be investigated further.

7.3 Recommendations

It is recommended that the following research be undertaken:

- A more detailed study must be done of the flux pulsations in the RSM using different stator-slot to flux-barrier ratios in the design. This is important as the flux pulsations affect the iron losses and thus the efficiency of the machine. The outcome of this study must show how the RSM must preferably be designed with respect to the stator-slot to flux-barrier ratio.
- A more detailed mechanical strength analysis of the high number of flux barrier RSM-rotor is required. This study is important for high speed operations and for mechanical shocks such as in locomotive applications.
- For a fixed number of stator slots and rotor flux barriers, the effect of the flux barrier position with respect to the stator slots (i.e. shifting the flux barriers with respect to the stator slots) on average torque and torque ripple of the RSM must be studied. This effect is not investigated in this thesis.
- The measurement system must be improved to accurately measure the differences in torque, efficiency and power factor of the low and high number of flux-barrier rotor RSMs at different speeds and current angles. The performance difference between these RSMs in the flux weakening region is specifically important.

Bibliography

[1] MJ Kamper, FS van der Merwe, S Williamson, *"Direct Finite Element Design Optimisation of the Cageless Reluctance Synchronous Machine"*, IEEE Trans. on Energy Conversion, Vol. 11, No. 3, September 1996, pp 547-553.

[2] XB Bomela, SK Jackson, MJ Kamper, *"Performance of Small and Medium Power Flux-barrier Rotor of Reluctance Synchronous Machine Drives"*, ICEM, September 1998, Vol. 1, pp 95-99.

[3] MJ Kamper, AT Mackay, *"Optimum Control of the Reluctance Synchronous Machine with a Cageless Flux Barrier Rotor"*, SAIEE Trans. , June 1995, pp 49-55.

[4] XB Bomela, MJ Kamper, *"Effect of Stator Chording and Rotor Skewing on Average Torque and Torque Ripple of Reluctance Synchronous machine"*, IEEE Africon, September/October 1999, Vol. 2, pp 687-690.

[5] MJ Kamper, *"Design Optimization of Cageless Flux Barrier Rotor Reluctance Synchronous Machine"*, PhD Thesis, University of Stellenbosch, December 1996.

[6] MJ Kamper, *"Design Criteria and development of a design program for squirrel-cage induction motors"* M.Eng. Dissertation (in Afrikaans), University of Stellenbosch, March 1987.

[7] A Fratta, GP Troglia, A Vagati and F Villata, *"Torque Ripple Evaluation of High-Performance Synchronous Machines"*, IEEE Industrial Applications Magazine, July/August 1995, pp 14-22.

[8] A Vagati, M Pastorelli, G Franceschini, SC Petrache, *"Design of Low-Torque-Ripple Synchronous Reluctance Motors"*, IEEE Trans. on Industrial Applications, Vol. 34, No. 4, July/August 1998.

[9] A Vagati, *"The Synchronous Reluctance Solution: A New Alternative in AC Drives"*, IEEE Trans. on Industrial Applications, 1994.

[10] TJE Miller, A Houton, C Cossar, DA Staton, *"Design of synchronous reluctance motor drive"* IEEE Trans. on Industrial Applications, IEEE Trans. on Industrial Applications, vol. 27, no. 4, July 1991.

[11] T Matsuo, TA Lipo, *"Field oriented control of synchronous reluctance machine "*, IEEE-PESC, pp 425-431, 1993.

[12] T Matsuo, TA Lipo, "*Rotor Design Optimization of Synchronous Reluctance Machine"*, IEEE Trans. on Energy Conversion, Vol. 9, No. 2, June 1994, pp 359-365.

[13] MJD Powell, *"An efficient method for finding the minimum of a function of several variables without calculating derivatives"*. Computer Journal, Vol. 7, pp 155-162, 1964.

[14] J Malan, MJ Kamper, PNT Williams, *"Reluctance Synchronous Machine Drive for Hybrid Electric Vehicle"*, IEEE International Symposium on Industrial Electronics Proceedings (ISIE'98), Vol. 2, July 1998, pp 367-372.

[15] XB Bomela, MJ Kamper, *"Electric Propulsion of Heavy Vehicles with Reluctance Synchronous Machine"*, LIW a division of Denel, Symposium 1998, October 1998.

[16] JJ Germisshuizen, K van der Westhuizen, MJ Kamper, *"Comparison of Reluctance Synchronous and Induction Motor Suburban Locomotive Drives"*, SAUPEC, pp 110-114, 1999.

[17] JJ Germisshuizen, *"Comparative Study of Reluctance Synchronous and Induction Machine Drives for Rail Traction"*, MSc Eng. Thesis, University of Stellenbosch, March 2000.

[18] I Boldea, ZX Fu, SA Nasar, *"Performance evaluation of axially-laminated anisotropic (ALA) rotor reluctance synchronous motors"* IEE-IAS Annual Meeting, Houston, Texas, October 1992, pp 212-218.

[19] T Spooner, "*Tooth pulsation in rotating machines"*, Trans A.I.E.E., 1924, Vol. 43, pp 252-261.

[20] KJ Binns, *"Calculation of some basic flux quantities in induction and other doubly-slotted electric machines"*, Proc. IEE, 1964, Vol. 111, No. 11, pp 1847-1858.

[21] KJ Binns and G Rowlands-Rees, *"Main-flux pulsations and tangential tooth-ripple forces in induction motors"*, Proc. IEE, 1975, Vol. 122, No. 3, pp 273-277.

[22] B Heller and V Hamata, *"Harmonic field effects in induction motors"*, Elsevier, 1977.

[23] FS van der Merwe, *"Some characteristics of magnetic field patterns in air-gaps with double-sided slotting"*, Archiv fur Elektrotechnik, 1979, Vol. 61, pp 327-336.

[24] R Mayer, H Mosebach, U Schroder, H Weh, *"Inverter-fed multiphase reluctance machine with reduced armature reaction and improved power density"*, ICEM (Munchem), Sept. 1986, Vol. 3, pp 1138-1141.

[25] I Marongiu and A Vagati, *"Improved modeling of a distributed aniso tropy synchronous reluctance machine"*, IEEE-IAS Annual Meeting (Dearborn, USA), Oct. 1991, Vol. 1, pp 238-243.

[26] L Xu, X Xu, TA Lipo, DW Novotny, *"Vector control of a synchronous reluctance motor including saturation and iron losses"*, IEEE Trans. on Industrial Applications, Vol. 27, No. 5, Sept. 1991, pp 977-985.

[27] JD Lavers, PP Binger and H Hollitscher, *"A simple method of estimating the minor loop hysteresis loss in thin laminations"*, IEEE Trans. on Magnetics, Sept. 1978, Vol. 14, No. 5, pp 386-388.

[28] JD Lavers, PP Biringer, *"Prediction of core losses for high flux densities and distorted flux waveforms"*, IEEE Trans. on Magnetics, Nov. 1976, Vol. 12, No. 6, pp 1053-1055.

[29] MJ Kamper, AF Volschenk, *"Effect of the rotor dimensions and cross magnetisation on L_d and L_q inductances of reluctance synchronous machine with cageless flux barrier rotor."*, IEE Electr. Power App., Vol. 141, No. 4, July 1994.

[30] RE Betz, TJE Miller, *"Apects of the control of synchronous reluctance machines"*, Proceedings European Power Electronics Conference, EPE'91, Florence, Sept. 6-9, 1991, pp 380-385.

[31] VB Honsinger, *"The inductances L_d and L_q of reluctance machines"*, IEEE Trans. PAS, Vol. 90, No. 1, Jan. 1971.

Appendix A

Pictures of the prototype RSM

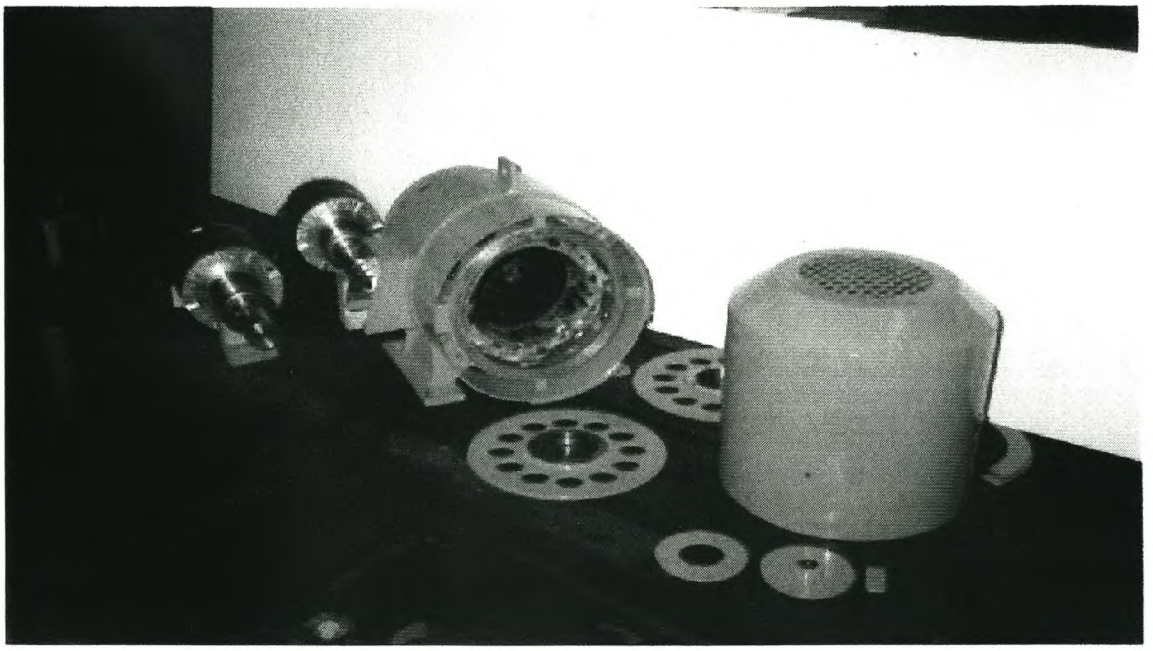

Figure A.1: Unassembled RSM (stator and two rotors)

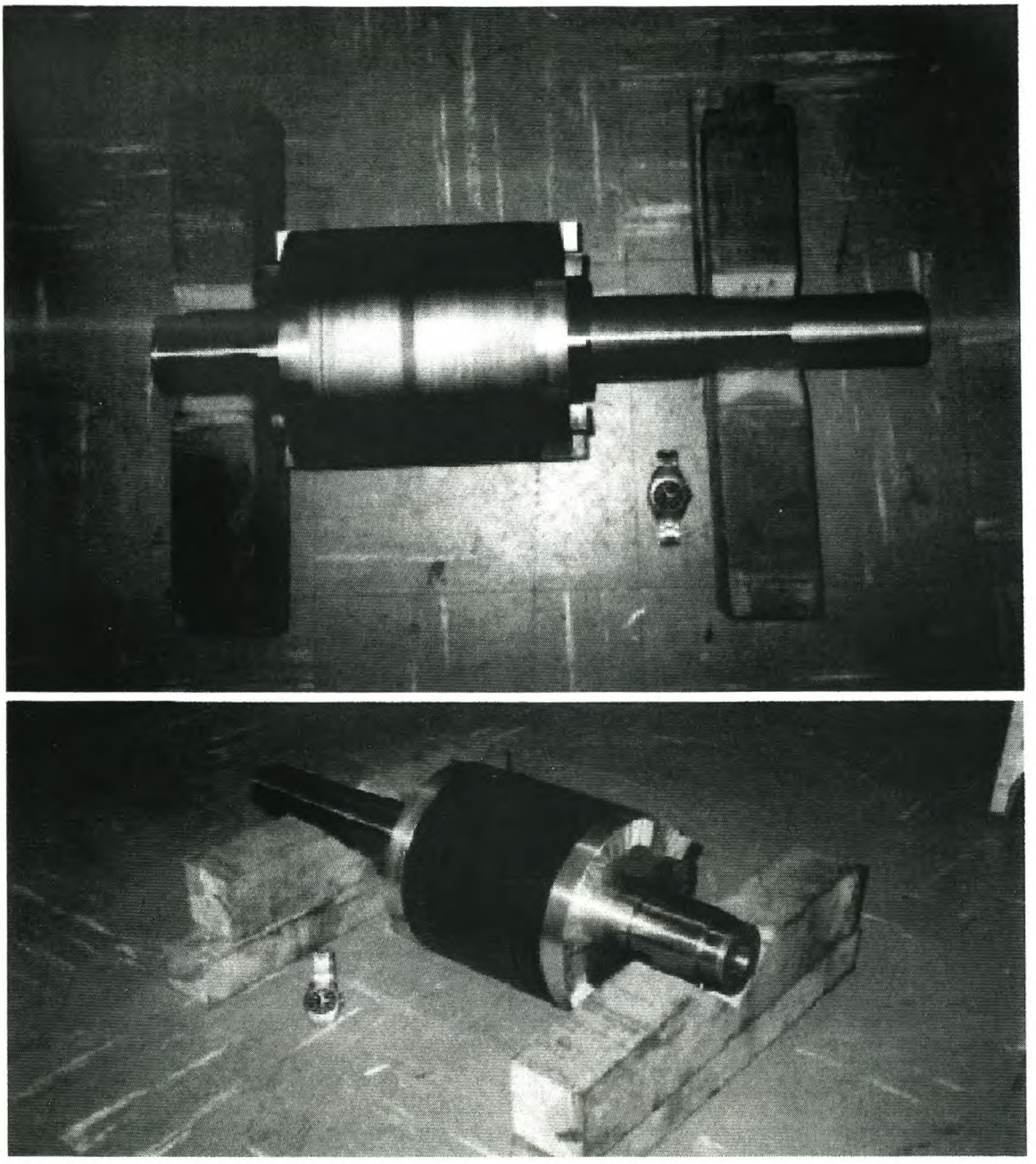

Figure A.2: Assembled transverse laminated rotor RSM (64-flux barrier rotor)

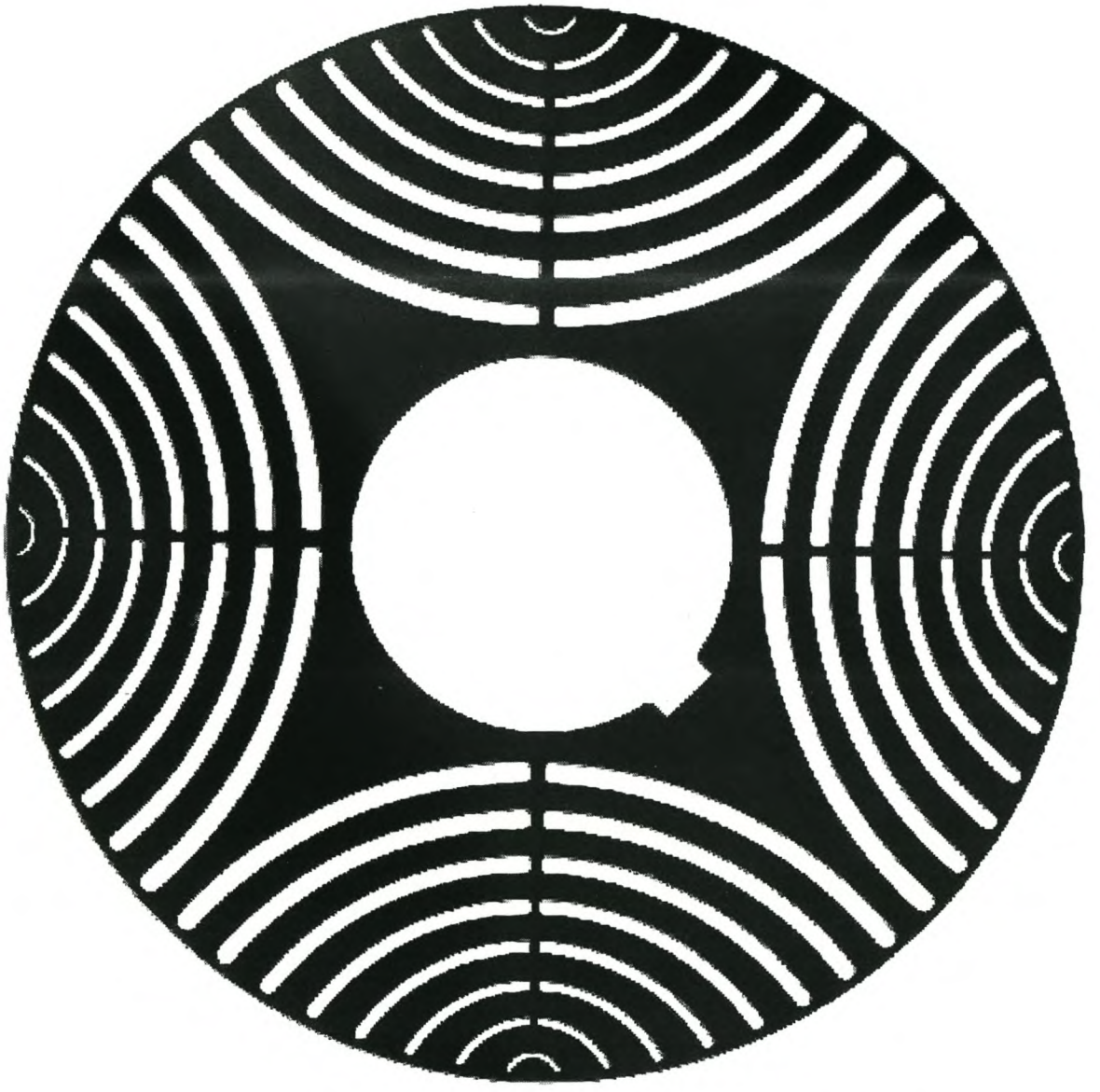

Figure A.3: Iron lamination of the 64-flux barrier rotor RSM

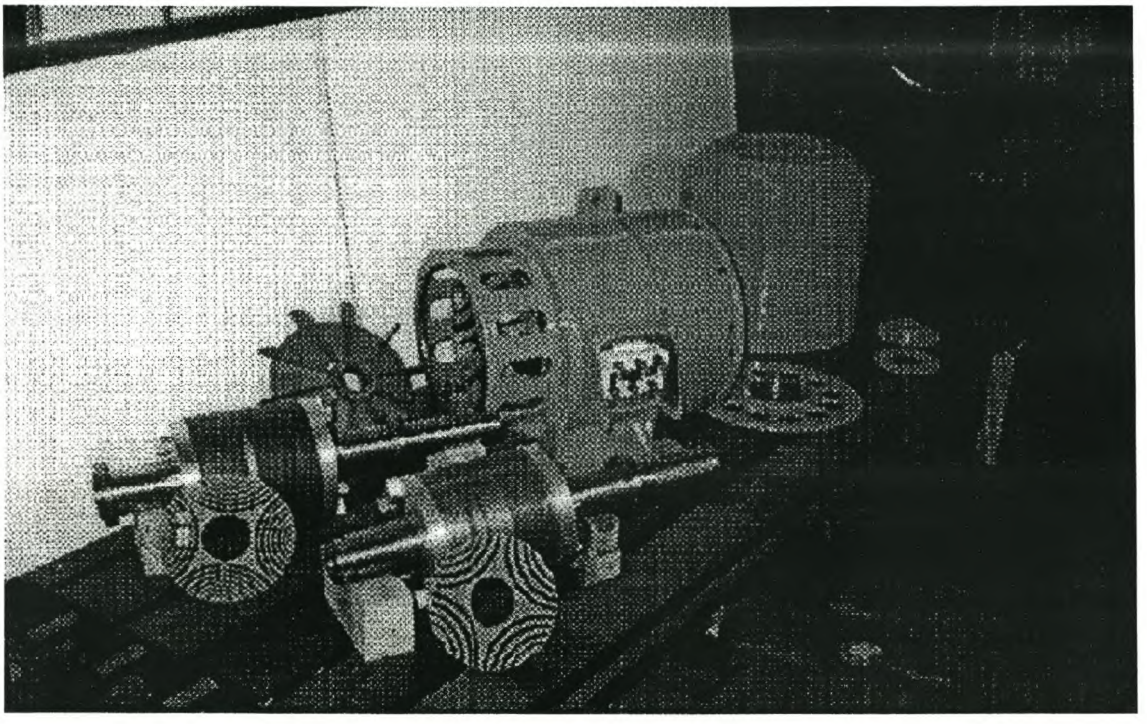

Figure A.4: Unassembled RSM stator with two rotors. The 32- and 64-flux -barrier laser cut iron laminations are shown in front.

Appendix B

Program for mesh generation

```
* ee_pol.f
*=================================================================================
*  sixteen barrier per pole rotor.
*=================================================================================
*
*  sub rotor_fbr generates the poly-shape for a reluctance  rotor-pole.
      subroutine rotor_fbr(nseg_pol,nspnts_pol,nstype_pol,x_pol,  y_pol,ro_od,ro_shfd,ro_cd,ro_bw,ro_ww,ro_rh,bw_nw,an_nw)
*_____________________________________________
*  Variable declaration
*  Start building the rotor-pole mesh:
*_____________________________________________
      nseg_pol=90
*  barrier type
        do i=1,39
         nstype_pol(i)=0
         if (i.eq.1.or.i.eq.6.or.i.eq.11.or.i.eq.16.or.i.eq.21.or.
     +       i.eq.26 .or.i.eq.31.or.i.eq.36) then
           nstype_pol(i)=250
         end if
        end do
        nstype_pol(36)=0
*  number of points for first 7 barriers:

       do i=0,6
        n=i*5
        nspnts_pol(n+1)=10
        nspnts_pol(n+2)=10
        nspnts_pol(n+3)=8
        nspnts_pol(n+4)=8
        nspnts_pol(n+5)=12
```

```
      end do

* barrier 8
      nspnts_pol(36)=10
      nspnts_pol(37)=10
      nspnts_pol(38)=8
      nspnts_pol(39)=12

* shaft and iron 1
      nspnts_pol(56)=7
      nspnts_pol(57)=12
      nspnts_pol(58)=8
      nspnts_pol(59)=8

* type for 40-90:
      do i=40,90
       !do i=56,90
        nstype_pol(i)=250
       if (i.eq.56) then
         nstype_pol(i)=0
       end if
      end do

*  first top-part:
      nspnts_pol(60)=13
      nspnts_pol(61)=11
      nspnts_pol(62)=10
* 2nd top-part:
      nspnts_pol(63)=11
      nspnts_pol(64)=9

* number of points in iron segments 65-82:
      do i=0,5
        n=i*3
        nspnts_pol(n+65)=10
        nspnts_pol(n+66)=8
        nspnts_pol(n+67)=8
      end do
* rib's:
      do i=40,55
       !nstype_pol(i)=0
       nspnts_pol(i)=10
      end do
```

```
* calculate angles for num points
* on airgap arc i.e. half pole pitch:
      num=56
      ainc=pi/4.0d0/dble(num)
      angl=ainc
      do i=1,num
        arc(i)=pi/4.0d0+angl
        angl=angl+ainc
      end do

* determine the points of flux barriers
* ---------------------------------

* determine thet and dist:

      angl=pi/180.0d0

      thet(1)=2.8125d0*angl
      thet(2)=8.4375d0*angl
      thet(3)=14.0625d0*angl
      thet(4)=19.6875d0*angl
      thet(5)=25.3125d0*angl
      thet(6)=30.9375d0*angl
      thet(7)=36.5625d0*angl
      thet(8)=42.1875d0*angl

* flux barrier distance:

      s_bw=0.0d0
      do n=2,7
        s_bw=s_bw+bw_nw(n)
      end do

      dist(1)=ro_shfd/2.0d0+bw_nw(1)/2.0d0+thet(1)*ro_od/2.0d0
      dist(8)=ro_od/2.0d0-thet(1)*ro_od/2.0d0
      a=dist(8)-dist(1)
      b=a-s_bw-bw_nw(1)/2.0d0-bw_nw(8)/2.0d0
      x=b/7.0d0
      dist(2)=dist(1)+(bw_nw(1)+bw_nw(2))/2.0d0+x
      dist(3)=dist(2)+(bw_nw(2)+bw_nw(3))/2.0d0+x
      dist(4)=dist(3)+(bw_nw(3)+bw_nw(4))/2.0d0+x
      dist(5)=dist(4)+(bw_nw(4)+bw_nw(5))/2.0d0+x
      dist(6)=dist(5)+(bw_nw(5)+bw_nw(6))/2.0d0+x
      dist(7)=dist(6)+(bw_nw(6)+bw_nw(7))/2.0d0+x
```

```
* Starting with points of eight barriers

      do j=1,8
       nx=5*j-4
        ny=nx+3
        nk=nx+4
        no_pol=3
        if (j.eq.8) then
          no_pol=2
          nk=nx+3
          ny=nx+2
        end if
       y_pol(nx,8)=dist(j)
       x_pol(nx,8)=0.0d0

* determine radius arcrad and aoff_y

       angl=pi/4.0d0+thet(j)
       c=ro_od/2.0d0-ro_r(j)-ro_b(j)/2.0d0
       call dpolrec(c,angl,arc_x,arc_y)
       angl=datan((arc_y-y_pol(nx,8))/arc_x)
       if (angl.ge.22.5d0*dg_rad) then
        a=arc_y-arc_x
        b=y_pol(nx,8)-a
        arcrad=b*dsin(112.5d0*dg_rad)/dsin(22.5d0*dg_rad)
        aoff_y=a+arcrad*sqrt2      ! ct
       else
        a=arc_x/dcos(angl)
        angl=pi/2.0d0-angl
        b=pi-2.0d0*angl
        arcrad=a*dsin(angl)/dsin(b)
        aoff_y=y_pol(nx,8)+arcrad
       end if

* points of region nk=5,10,15,20,25,30,35,39

       nz=nk
       x_pol(nz,12)=arc_x
       y_pol(nz,12)=arc_y
       call drecpol(arc_x,arc_y-aoff_y,a,angl)
       if (dabs(angl).le.45.0d0*dg_rad) then
        angl=-45.0d0*dg_rad
       end if
```

```
      a=ro_b(j)/2.0d0
      b=angl
      ainc=pi/10.0d0
      do i=1,11
       call dpolrec(a,b,arc_x,arc_y)
       x_pol(nz,i)=x_pol(nz,12)+arc_x
       y_pol(nz,i)=y_pol(nz,12)+arc_y
       b=b+ainc
      end do
```

* points of region nx (regions 1,6,11,16,21,26,31,36).

```
      x_pol(nx,1)=ro_w(j)+0.0d0
      y_pol(nx,1)=y_pol(nx,8)-ro_b(j)/2.0d0
      x_pol(nx,2)=ro_w(j)
      y_pol(nx,2)=y_pol(nx,8)-ro_b(j)/4.0d0
      x_pol(nx,3)=x_pol(nx,2)
      y_pol(nx,3)=y_pol(nx,8)
      x_pol(nx,4)=ro_w(j)
      y_pol(nx,4)=y_pol(nx,8)+ro_b(j)/4.0d0
      x_pol(nx,5)=x_pol(nx,1)
      y_pol(nx,5)=y_pol(nx,8)+ro_b(j)/2.0d0
      x_pol(nx,6)=0.0d0
      y_pol(nx,6)=y_pol(nx,5)
      x_pol(nx,7)=0.0d0
      y_pol(nx,7)=y_pol(nx,4)
      x_pol(nx,9)=0.0d0
      y_pol(nx,9)=y_pol(nx,2)
      x_pol(nx,10)=0.0d0
      y_pol(nx,10)=y_pol(nx,1)
```

* points for region nx+1 (i.e. the regions 2,7,12,17,22,27,32,37).

```
      nz=nx+1
      i=5
      do n=3,7
       x_pol(nz,n)=x_pol(nx,i)
       y_pol(nz,n)=y_pol(nx,i)
       i=i-1
      end do
      arc_x=x_pol(nk,11)
      arc_y=y_pol(nk,11)-aoff_y
      call drecpol(arc_x,arc_y,a,b)
      arc_x=x_pol(nz,3)
```

```
      arc_y=y_pol(nz,3)-aoff_y
      call drecpol(arc_x,arc_y,a,angl)
      ainc=(dabs(angl-b))/(2.0d0*dble(no_pol))
      do i=2,1,-1
       angl=angl+ainc
       a=arcrad-ro_b(j)/2.0d0
       if (dabs(angl).ge.40.0d0*dg_rad) then
        call dpolrec(a,angl,arc_x,arc_y)
        x_pol(nz,i)=arc_x
        y_pol(nz,i)=arc_y+aoff_y
        a=arcrad+ro_b(j)/2.0d0
        call dpolrec(a,angl,arc_x,arc_y)
        x_pol(nz,10-i)=arc_x
        y_pol(nz,10-i)=aoff_y+arc_y
       else
        k=no_pol*2-2
        a=(x_pol(nk,11)-x_pol(nz,i+1))/dble(i+k)
        b=(x_pol(nk,1)-x_pol(nz,9-i))/dble(i+k)
        x_pol(nz,i)=x_pol(nz,i+1)+a
        y_pol(nz,i)=y_pol(nz,i+1)+a
        x_pol(nz,10-i)=x_pol(nz,9-i)+b
        y_pol(nz,10-i)=y_pol(nz,9-i)+b
       end if
      end do
      x_pol(nz,10)=(x_pol(nz,1)+x_pol(nz,9))/2.0d0
      y_pol(nz,10)=(y_pol(nz,1)+y_pol(nz,9))/2.0d0
      if (j.eq.8) goto 327

* points for region nx+2 (regions 3,8,13,18,23,28,33,38)

      nz=nx+2
      x_pol(nz,3)=x_pol(nx+1,1)
      y_pol(nz,3)=y_pol(nx+1,1)
      x_pol(nz,4)=x_pol(nx+1,10)
      y_pol(nz,4)=y_pol(nx+1,10)
      x_pol(nz,5)=x_pol(nx+1,9)
      y_pol(nz,5)=y_pol(nx+1,9)
      do i=2,1,-1
       angl=angl+ainc
       a=arcrad-ro_b(j)/2.0d0
       if (dabs(angl).ge.40.0d0*dg_rad) then
      call dpolrec(a,angl,arc_x,arc_y)
      x_pol(nz,i)=arc_x
      y_pol(nz,i)=arc_y+aoff_y
```

```
      a=arcrad+ro_b(j)/2.0d0
      call dpolrec(a,angl,arc_x,arc_y)
      x_pol(nz,8-i)=arc_x
      y_pol(nz,8-i)=aoff_y+arc_y
     else
      a=(x_pol(nk,11)-x_pol(nz,i+1))/dble(i+2)
      b=(x_pol(nk,1)-x_pol(nz,7-i))/dble(i+2)
      x_pol(nz,i)=x_pol(nz,i+1)+a
      y_pol(nz,i)=y_pol(nz,i+1)+a
      x_pol(nz,8-i)=x_pol(nz,7-i)+b
      y_pol(nz,8-i)=y_pol(nz,7-i)+b
     end if
    end do
    x_pol(nz,8)=(x_pol(nz,1)+x_pol(nz,7))/2.0d0
    y_pol(nz,8)=(y_pol(nz,1)+y_pol(nz,7))/2.0d0

* points for region ny:

 327 nz=ny
    lcn=0
    if (j.eq.8) lcn=2
     x_pol(nz,3)=x_pol(ny-1,1)
     y_pol(nz,3)=y_pol(ny-1,1)
     x_pol(nz,4)=x_pol(ny-1,8+lcn)
     y_pol(nz,4)=y_pol(ny-1,8+lcn)
     x_pol(nz,5)=x_pol(ny-1,7+lcn)
     y_pol(nz,5)=y_pol(ny-1,7+lcn)
     angl=angl+ainc
     a=arcrad-ro_b(j)/2.0d0
     if (dabs(angl).ge.40.0d0*dg_rad) then
      call dpolrec(a,angl,arc_x,arc_y)
      x_pol(nz,2)=arc_x
      y_pol(nz,2)=arc_y+aoff_y
      a=arcrad+ro_b(j)/2.0d0
      call dpolrec(a,angl,arc_x,arc_y)
      x_pol(nz,6)=arc_x
      y_pol(nz,6)=aoff_y+arc_y
     else
      a=(x_pol(nk,11)-x_pol(nz,3))/2.0d0
      b=(x_pol(nk,1)-x_pol(nz,5))/2.0d0
      x_pol(nz,2)=x_pol(nz,3)+a
      y_pol(nz,2)=y_pol(nz,3)+a
      x_pol(nz,6)=x_pol(nz,5)+b
      y_pol(nz,6)=y_pol(nz,5)+b
```

```
      end if
      x_pol(nz,1)=x_pol(nk,11)
      y_pol(nz,1)=y_pol(nk,11)
      x_pol(nz,8)=x_pol(nk,12)

      y_pol(nz,8)=y_pol(nk,12)
      x_pol(nz,7)=x_pol(nk,1)
      y_pol(nz,7)=y_pol(nk,1)

     end do
*_____

*    points of regions 40-55: the rib-points.

      nx=40
      do j=1,8
      nk=5*j
      if (j.eq.8) then
       nk=39
      end if

      a=pi/4.0d0+thet(j)
      b=a-(sqrt2*ro_b(j)/ro_od)
      ainc=(a-b)/3.0d0
      angl=b
      do n=1,2
       do i=8,10
        call dpolrec(ro_od/2.0d0,angl,arc_x,arc_y)
        x_pol(nx,i)=arc_x
        y_pol(nx,i)=arc_y
        angl=angl+ainc
       end do
       nx=nx+1
      end do
      nx=nx-1
      call dpolrec(ro_od/2.0d0,angl,arc_x,arc_y)
      x_pol(nx,1)=arc_x
      y_pol(nx,1)=arc_y

      nx=nx-1
      x_pol(nx,1)=x_pol(nx+1,8)
      y_pol(nx,1)=y_pol(nx+1,8)
      ny=6
      do i=3,6
```

```
      x_pol(nx,i)=x_pol(nk,ny)
      y_pol(nx,i)=y_pol(nk,ny)
      ny=ny-1
      end do
      x_pol(nx,2)=(x_pol(nx,1)+x_pol(nx,3))/2.0d0
      y_pol(nx,2)=(y_pol(nx,1)+y_pol(nx,3))/2.0d0
      x_pol(nx,7)=(x_pol(nx,6)+x_pol(nx,8))/2.0d0
      y_pol(nx,7)=(y_pol(nx,6)+y_pol(nx,8))/2.0d0

      ny=9
      nx=nx+1
      do i=3,5
      x_pol(nx,i)=x_pol(nk,ny)
      y_pol(nx,i)=y_pol(nk,ny)
      ny=ny-1
      end do
      x_pol(nx,2)=(x_pol(nx,1)+x_pol(nx,3))/2.0d0
      y_pol(nx,2)=(y_pol(nx,1)+y_pol(nx,3))/2.0d0
      x_pol(nx,6)=x_pol(nx-1,3)
      y_pol(nx,6)=y_pol(nx-1,3)
      x_pol(nx,7)=x_pol(nx-1,2)
      y_pol(nx,7)=y_pol(nx-1,2)
      nx=nx+1

      end do
*=======================================================================
*  standard stator slot shape:     refer  to the program code by Kamper (1996) [5].
*=======================================================================
```

Appendix C

Program for the solver

```
*     (c) af volschenk, 1994
*     contact: MJ Kamper, Dept e/e Eng, Stellenbosch, 7600
*     tel:021-808-4457/3890
*     revision history by Bomela XB* as from the 16 February 1998
*     design optimisation
*     calculations based on flux linkages: solvec.f
*-------------------------------------------------------+
* variable declarations
*
      SUBROUTINE eesolv(xpar,ypar)
*-------------------------------------------------------
  103 format('')
  131 format(1F5,6F7.3,3F9.3,1F7.3)
  120 format(1F5.1)
  121 format(1F5.1,2F9.3)
  122 format(3F7.3)
  151 format('8 barrier')
*-------------------------------------------------------
      pi=4.0d0*datan(1.0d0)
      sqrt2=dsqrt(2.0d0)
*-------------------------------------------------------
*       INPUT ROTOR AND STATOR PARAMETERS
*-------------------------------------------------------
      do mem=1,1
       write(22,103)
       write(22,120) dble(mem)
       bw=4.4068d0*0.001d0
       m=-0.09296d0
       do n =1,8
        bw_nw(n)=(m*(n-1)+1)*bw
```

```
      end do

       t_wid=7.63d0*0.001d0
       st_yh=36.15d0*0.001d0
       st_id=198.94d0*0.001d0
       alpha=65.0d0
       ro_obw=1.0d0
      ro_bw=5.6d0*0.001d0
       ro_cw=1.0d0
       airg_l=0.00062d0
       ro_od=st_id-2.0d0*airg_l
       ro_rl=ro_bw

* the other rotor pole dimensions stay the same:
       n_ro_st=4
       ro_shfd=0.07d0
       ro_ww=0.002d0
       ro_rh=0.0013d0
       ro_wl=ro_ww/2.0d0
       ro_bl=.02

       if (mem.eq.2) ro_rh=0.00005d0

* and save to data file
       rs_file='mjk_nbr.dat'
       rs_type='fbr'

      call save_rslot(rs_file,rs_type,ro_od,n_ro_st,ro_ww,ro_obw,
     &   ro_shfd,ro_cd,ro_cw,ro_bd,ro_bw,ro_wl,ro_bl,ro_rh,ro_ang,
     &   ro_rl,an_nw,bw_nw)

c ------------------------------------
*      INPUT STATOR PARAMETERS
* ------------------------------------
*
      ss_type='sss'
      n_st_st=48
      st_od=0.34d0
      st_slh=0.5d0*(st_od-st_id)-st_yh

* these stay the same:
      st_gw=0.0057d0*st_id/0.309d0
      if (mem.eq.3) st_gw=6.0d0*0.001d0
```

```
      st_sht=0.001d0
      st_shs=0.0016d0

* calculate further (pp.2):
      a_slt=dble(n_st_st)
      st_tw=(pi*(st_id+2.0d0*(st_sht+st_shs))-a_slt*t_wid)/a_slt
      st_bw=(pi*st_od-2.0d0*pi*st_yh-t_wid*a_slt)/(a_slt+pi)
      st_shb=st_slh-st_shs-st_sht-0.5d0*st_bw

* other parameters:
      stack=0.97d0
      f=66.60
      v_line=380.0
      temp=120.0
*     cur_den=6.0d0
      fill_f=0.75
      w=0.175d0*stack
*     p_cu=13500.0d0
      p_cu=25000.0d0
      p_wf=300.0d0
      l_ce=0.27d0
*
* and save to data file

      ss_file='mjk_ss1.dat'
      call save_sslot(ss_file,ss_type,n_st_st,st_od,st_id,st_gw,
     &   st_bw,st_tw,st_sht,st_shs,st_shb)

*     goto 133

* ------------------------------------------
*     MAKE THE MESH AND START WITH CALCULATIONS
* ------------------------------------------
*
      ofile='temp/mjk2.pol'
      ifile='mjk2.fpl'
          def_file='mjk2.def'

* make the mesh and save to mjk2.fpl
*
          CALL ee_as(def_file,ofile,rat)
      CALL ee_pmesh(ofile,ifile,nelm,nnode)
*
* and then do the preprocessing
```

```
*
      CALL ee_pre(def_file,nprof)
*
* Files for solver

      call sreadmesh(fname,nde,nelm,nnode,x,y,node,itype,testa,
     &   nlines,line,neigh)
*
* winding info
*
      call read_sw(w_file,n_st_sp,nw_it,nw_f,nw_t,nw_ci,wn,
     &   rw,end_w,ns)
*
* convert the X_end-winding to inductance
* calculate l_end separately
*
      do i=1,3
        end_w(i)=end_w(i)/2.0/pi/f
      end do
*
* leakage inductance per phase: not used
     l_leak=0.00489
*
*
* number of poles
     np=n_st_st/n_st_sp
* number of pole pairs
     nppole=np/2
* number of stator slots per pole?
     nslots=n_st_rq
* number of stator slots per pole per phase
     ns_pph=nslots/ns
* windingfactors for nth harmonic, cth/12 pitch
     qwn=0.958
* number of pole pitches in model? Currently only 1 for neg. periodicity
     npp=n_st_rq/n_st_sp
* spline and generator
     call acs_spline(bh_file)

* axial length to meters?
     ax=w
* skew in bars? 2.0*pi/n_st_st?: not used
     skew=skew_b*pi/dble(n_st_st)
*
```

```
* re timestepping: not used
      big_t=36.0d0
      small_t=4.0d0
*
* Inductance calculations ? 0=no, 1=yes, 2=just read in from ind
      ind_do=0

* DC actual  resistances: calculate r_s separately
      do i=1,ns
        do j=1,ns
          r(i,j)=0.0d0
        end do
      end do

      do i=1,ns
        r(i,i)=rw(i)
      end do

*-----------------------------------------------------------
* program main body
* ----------------------------------------------------------
*       DATA read in from mesh & prepro
      open (9,file='temp/age.ren',form='formatted')
      rewind 9
*
* circuit numbering convention
*       phase a 1
*       phase b 2
*       phase c 3
*
* the 'physical coils' present are a bit more tricky
*
        ic_typ(1)=1
        ic_typ(2)=2
        ic_typ(3)=3
        ncoil=3
*
* default reluctivities
* Take peak value of fundamental airgap flux density = 0.8 Tesla

        nc_turns(1)=6
        np_cir=2

* Calculate number of turns in series per phase (double layer)
```

```
      nphase=2.0d0*nc_turns(1)*ns_pph*nppole/np_cir

* Calculate the endwinding inductance: for now only double layer
      l_end=57.83d0*st_id*(nphase**2)*1.0d-8

* Calculate the per phase stator resistance at 120 deg.C
* See [5] on page 91 Appedix A, formula A.1 & A.2

      a_cu=acoil(1)*0.82d0
      a_sc=(pi/4.0)*(0.93**2)*fill_f*a_cu/nc_turns(1)
      r_s=2.0d0*nphase*17.0d-9*1.39d0*(w/stack+l_ce)/a_sc/np_cir

      !************************************************************
      ! PROGRAM:  Calculate flux linkages with  skew
      !************************************************************

      ! phase currents as a function of current angle "alpha" and rotor position "theta-m" in mechanical degrees from phase a
      ! to magnetic axis anti-clockwise

      do icurrent=10,10
       ! c_peak1=78.0*1/3, 2/3, 1.0, 1.33, 1.66, 2.0, 2.308 p.u.
       do c_peak1 = 195,195
         c_peak=(sqrt2*dsqrt(p_cu/r_s/3.0d0))/np_cir
        do ialpha = 65,65
         alpha=ialpha*pi/180.0d0
         cur_id=c_peak*dble(np_cir)*dcos(alpha)
         cur_iq=c_peak*dble(np_cir)*dsin(alpha)

         ! set the off-set rotor-angle with the rotor q-axis on the magnetic axis of phase a

         th_off=-15.0d0*pi/180.0d0

         ! Rotate machine if wanted:
         step_angl=1.0d0*pi/180.0d0
         open (2, FILE="results/deltaxy.res", form='formatted')
         rewind 2
         read (2,*) dy1, dx1, dy2, dx2
         read (2,*) del y1, delx1, dely2, delx2
         read (2,*) dy, dx
         read (2,*) dely, delx
         close (2,status= 'keep')

         theta_m=-0.5d0*pi/180.0d0
         do ithet_m=9,9
```

```
      theta_m=theta_m+0.5d0*pi/180.0d0

      c_cur(1)=c_peak*dsin(nppole*theta_m+alpha)
      c_cur(2)=c_peak*dsin(nppole*theta_m+alpha+2.0d0*pi/
     &     3.0d0)
      c_cur(3)=c_peak*dsin(nppole*theta_m+alpha-2.0d0*pi/
     &     3.0d0)
      cur(1)=c_cur(1)
      cur(2)=c_cur(2)
      cur(3)=c_cur(3)

      ! take ks slice(s) over slot pitch.
      ks=5
      d_slice=2.0d0*pi/dble(n_st_st)/dble(ks)
      !d_slice=0.0d0

     T = 0.0d0
      T100 = 0.0d0
      lamda_dm=0.0
      lamda_qm=0.0
     do i=1,3
       flink(i)=0.0
     end do
     do ik=1,3
       do jk=1,3
         mss(ik,jk)=0.0
       end do
     end do
     !=====================================
     ! calculate parameters at each slice position
     !————— START SLICE ———
     !=====================================

     do i=1,ks
       if (ks.eq.1) then
         dtheta=theta_m+th_off
         alpha_i=alpha
       else if (ks.eq.5) then
         dtheta=dble(i-ks+2)*d_slice+theta_m+th_off
         alpha_i=dble(3-i)*d_slice*nppole+alpha
       end if

       call step(dtheta,sraz,nfour,terms,an,bn,nrs,nt,
     &     ah,ap,bh,bp,la,thao)
```

```
      call nonlinear(neq,nelm,nnode,nprof,nraz,v0,ar,nd,
&       node,razpnt,itype,jdiag,s,sraz,rel,c_cur,a,x,y,
&       razind,nppole,acoil,nc_turns,w,ms,np,ns,zp,
&       nlines,line,neigh,bcur)

      ! just do position 1 again for accuracy
      if (ithet_m.eq.1) then
       call nonlinear(neq,nelm,nnode,nprof,nraz,v0,ar,nd,
&        node,razpnt,itype,jdiag,s,sraz,rel,c_cur,a,x,y,
&        razind,nppole,acoil,nc_turns,w,ms,np,ns,zp,
&        nlines,line,neigh,bcur)
      end if

      ! calculating Bflux on the stator tooth

      By2=(a(1786)-a(1864))/t_wid    ! top
      By1=(a(1778)-a(1854))/t_wid    ! bottom

      !if (mem.eq.3) then
      !  By1=(a(1778)-a(1854))/t_wid
      !  By2=(a(1786)-a(1864))/t_wid
      !end if

      ! calculating a flux density at one point(region 91)
      ! Bx and By flux densities.

      B_x=(a(462)-a(466))/dy1
      B_y=(a(463)-a(461))/dx1

      ! calculating a flux density at one point(region 93)
      ! Bx and By flux densities.

      B_xx=(a(469)-a(473))/dely2
      B_yy=(a(472)-a(474))/delx2

      ! calculate torque
      call torque(rrad,srad,torq1,100,nppole,nrs,nraz,ax,
&       a,an,bn,razind)
      T100 = T100 + torq1
       call torque(rrad,srad,torq1,1,nppole,nrs,nraz,ax,
&       a,an,bn,razind)
      T = T + torq1

      hoek=theta_m*180.0d0/pi
```

```
*           write (22,121) hoek,B_y,B_x,B_yy,B_xx,By1,By2,flink(1),torq1
*-------------------------------------------------------------------
* Air-gap flux densities, flux linkages and induce EMF are now determined of the fundamental.  On Razek airgap points the cc
* Bgap(radial) = 1/r.dA/dtheta is calculated and then the fundamental Bgap using Foerier analysis.  Ephase contains
* the value obtained by using the fundamental Bgap
*-------------------------------------------------------------------

        open (10, FILE="results/bgap.res", form='formatted')
        rewind 10
        do ib=(nrs+1),nt
         bgap(ib)=1/(st_id/2.)/(dabs(rthet(ib+1)-
     &       rthet(ib)))*(A(razind(ib+1))-A(razind(ib)))
         write (10,125) ((rthet(ib+1)+rthet(ib))/2.0),
     &       bgap(ib)
        end do
125      format(2F10.5)
        close (10,STATUS='KEEP')

       ! ================================================
       !     FINAL CALCULATIONS
       ! ================================================

       ! Calculate: from airgap flux:

       T      = T/dble(ks)
       T100   = T100/dble(ks)
       lamda_s  = dsqrt(lamda_dm**2 + lamda_qm**2)
       fluxang  = datan(lamda_qm/(lamda_dm + 1.0d-12))
       if (alpha.gt.pi/4.0.and.fluxang.lt.0.0) then
        fluxang  = fluxang + pi
       end if
       fl_am  = lamda_s*dsin(nppole*theta_m + fluxang)

       fluxang=fluxang*180.0d0/pi
       Ephase=2.0*pi*50./sqrt2*lamda_s

       ! Calculate the dq-axis inductances from airgap flux:

       l_d  = lamda_dm/(cur_id + 1.0d-12)
       l_q  = lamda_qm/(cur_iq + 1.0d-12)
       Te   = 3.0d0*(l_d-l_q)*cur_id*cur_iq
       If (cur_iq.eq.0.0) l_q  = 0.0
       If (cur_id.eq.0.0) l_d  = 0.0
```

```
      ! Calculate d- and q-axis L, flink, Erms (p. ...)

      do ikk = 1,3
       flink(ikk) = flink(ikk)/dble(ks)/dble(np_cir)
      end do

      l_leak = (flink(1)-fl_am)/(c_cur(1)*np_cir) + 0.001d0
      l_d    = l_d + l_leak
      l_q    = l_q + l_leak

      fl_ab  = flink(1) - flink(3)
      fl_bc  = flink(3) - flink(2)
      fl_ca  = flink(2) - flink(1)
      xf     = nppole*theta_m + 30.0d0*pi/180.0d0
      yf     = nppole*theta_m - 90.0d0*pi/180.0d0
      beta   = datan((fl_ab*dsin(yf) - fl_bc*dsin(xf))/
     &          (fl_bc*dcos(xf) - fl_ab*dcos(yf)))
      f_peak = fl_ab/(dsqrt(3.0d0)*dsin(xf + beta))
      l_df   = 1000.0d0*(f_peak*dcos(beta)/cur_id + l_end)
      l_qf   = 1000.0d0*(f_peak*dsin(beta)/cur_iq + l_end)
      Tef    = 3.0d0*(l_df - l_qf)*cur_id*cur_iq/1000.0d0
      e_d    = f_peak*dcos(beta + pi/2.0d0)*omegas
      e_q    = f_peak*dsin(beta + pi/2.0d0)*omegas
      e_rms  = dsqrt(e_d**2 + e_q**2)/sqrt2

      ! ---------------------------------------
      ! Calculate iron core loss resistance r_c (pp. 55-58)
      ! ---------------------------------------

      ! Calculate mass of teeth and yoke:

      ar_slot = 2.0d0*acoil(1)*50.0/48.0+0.5*(st_gw+st_tw)*
     &    st_shs+st_gw*st_sht
      mass_y  = 7880.0d0*w*(pi/4.0)*(st_od**2-(st_id+2.0*
     &    st_slh)**2)
      mass_t  = 7880.0d0*w*((pi/4.0)*((st_id+2.0*
     &    st_slh)**2-st_id**2)-n_st_st*ar_slot)

      ! Calculate maximum flux density in teeth and yoke:
      flux_pp  = e_rms/(4.44d0*f*nphase*qwn)
      bp_air   = flux_pp*dble(np)/(2.0d0*st_id*w)
      t_pitch  = pi*st_id/a_slt
      bp_t     = bp_air*t_pitch/t_wid
      bp_y     = flux_pp/(2.0d0*st_yh*w)
```

```
! Calculate iron core loss:
const  = ((bp_t**2)*mass_t+(bp_y**2)* mass_y)
p_core = 0.0337d0*(f**1.32)*const

! Calculate core loss resistance:
r_c  = 3.0d0*e_rms**2/p_core

! ---------------------------
! calculate kVA, powerfactor, efficiency
! ---------------------------
cur_id1  = cur_id+e_d/r_c
cur_iq1  = cur_iq+e_q/r_c

cur_ang = datan(cur_iq1/(cur_id1 + 1.0d-12))*180.0d0/pi

i_rms  = dsqrt(cur_id1**2 + cur_iq1**2)/sqrt2

! Calculating the terminal voltage
v_d    = e_d - omegas*cur_iq1*(l_end) + r_s*cur_id1
v_q    = e_q + omegas*cur_id1*(l_end) + r_s*cur_iq1
v_rms  = dsqrt(v_d*v_d + v_q*v_q)/sqrt2
kva    = 3.0d0*i_rms*v_rms/1000.0d0

! Calculating power factor
num    = datan(dabs(v_d/v_q))
cur_r  = cur_id1/cur_iq1
p_fact = dcos((num) + datan(cur_r))
*       print *,'num, currentratio, pf  =',num,cur_r,p_fact

T_out  = Tef-p_wf*dble(nppole)/omegas

! Calculate th copper losses

! i_rms  =  c_peak*3.0d0/sqrt2
p_cu   =  3.0d0*(i_rms**2)*r_s

! Calculate the efficiency in terms of losses

p_out =  omegas*T/dble(nppole)-p_wf

cur_den = i_rms/(a_sc*1.0d + 6*dble(np_cir))
p_loss  = p_cu + p_core + p_wf
p_in    = p_out + p_loss
```

```
      eff    = p_out/p_in

      ! ---------------
      ! results to main program
      ! ---------------

      Tr=640.0d0
      pry=10500.0d0

      ypar(1)=ithet_m
      ypar(2)=cur_ang
      ypar(3)=p_fact
      ypar(4)=T
      ypar(5)=T100
      ypar(6)=p_out
      ypar(7)=p_in
      ypar(8)=eff*100.0d0
      ypar(9)=p_core/1000.0d0
      ypar(10)=p_cu/1000.0d0
      ypar(11)=qwn

      ! Write to file:performb.res

      write(22,131) ypar(1),ypar(2),ypar(3),ypar(4),
     &     ypar(5),ypar(6),ypar(7),ypar(8),ypar(9),ypar(10),
     &     ypar(11)

      write (22,121) ithet_m,T,torq1

*     fl_ab=flink(1)
*     write (22,121) hoek,B_y,B_x,B_yy,B_xx,By1,By2,fl_ab,torq1
*     write (22,121) hoek,B_y,B_x,B_yy,B_xx,By1,By2,ithet_m,torq1

      print *,' At Pcu  = 25kW '
      print *,' Eff    =',eff*100.0d0
      print *,' pf     =',p_fact
      print *,' p_loss =',p_loss
      print *,' kVA    =',kVA
      print *,' T      =',T
      print *,' T100   =',T100

    end do        ! end of rotate ithet_m
   end do         ! end of alpha
  end do          ! end of c_peak1
```

```
    end do          ! end of icurrent
   end do           ! end of mem

   close (22,status='keep')

   out_file='blug.fpl'
   call save_dth(out_file,nde,nelm,nnode,x,y,node,itype,
  &  nlines,line,neigh,a,dtheta,rr)

133 continue
   RETURN
   END

   ! end of eesolve program
```